https://ntrs.nasa.gov/search.jsp?R=19690014322 2020-03-12T03:46:34+00:00Z

General Disclaimer

One or more of the Following Statements may affect this Document

- This document has been reproduced from the best copy furnished by the organizational source. It is being released in the interest of making available as much information as possible.

- This document may contain data, which exceeds the sheet parameters. It was furnished in this condition by the organizational source and is the best copy available.

- This document may contain tone-on-tone or color graphs, charts and/or pictures, which have been reproduced in black and white.

- This document is paginated as submitted by the original source.

- Portions of this document are not fully legible due to the historical nature of some of the material. However, it is the best reproduction available from the original submission.

Produced by the NASA Center for Aerospace Information (CASI)

CR 86140

RESEARCH INTO THE FEASIBILITY OF THIN METAL AND OXIDE FILM CAPACITORS

by

M. E. Browning

G. V. Jorgenson

W. H. Graves

N 69-23700

FACILITY FORM 602

(ACCESSION NUMBER)	(THRU)
81	1
(PAGES)	(CODE)
CR-86140	09
(NASA CR OR TMX OR AD NUMBER)	(CATEGORY)

June 1968

Interim Scientific

Prepared Under Contract No. NAS 12-551 by

NORTH STAR RESEARCH AND DEVELOPMENT INSTITUTE

3100 THIRTY-EIGHTH AVENUE SOUTH • MINNEAPOLIS, MINNESOTA 55406

for

Electronics Research Center

NATIONAL AERONAUTICS AND SPACE ADMINISTRATION

Distribution of this report is provided in the interest of information exchange and should not be construed as endorsement by NASA of the material presented. Responsibility for the contents resides with the organization that prepared it.

Dr. F. C. Schwarz
Technical Monitor
NAS 12-551
Electronics Research Center
575 Technology Square
Cambridge, Massachusetts 02139

"Requests for copies of this report should be referred to:

NASA ~~Scientific and Technical Information Facility~~
P. O. ~~Box 33, College Park, Maryland 20740~~"
CFS71

RESEARCH INTO THE FEASIBILITY OF THIN METAL AND OXIDE FILM CAPACITORS (U)

by

M. E. Browning
G. V. Jorgenson
and
W. H. Graves

June 1968

Prepared Under Contract No. NAS 12-551

by

NORTH STAR RESEARCH AND DEVELOPMENT INSTITUTE
Minneapolis, Minnesota

Electronics Research Center
NATIONAL AERONAUTICS AND SPACE ADMINISTRATION

TABLE OF CONTENTS

	Page
SUMMARY	1
INTRODUCTION	2
EXPERIMENTAL PROCEDURE	3
Material Selection	3
Screening Studies	3
Prototype Trials	5
Deposition Process Studies	6
Initial Deposition Studies	8
Studies in Ultrahigh Vacuum	10
Capacitor Development	11
Electrodes	11
Dielectrics	11
Film Thickness Measurements	12
Examination of Capacitors and Substrates	13
Multilayered Capacitor Preparation	14
Electrical Tests	15
Test Equipment	17
Test Results	17
Property Review	23
CONCLUSIONS AND RECOMMENDATIONS	25
REFERENCES	26
FIGURES	28
APPENDIX	

LIST OF FIGURES

		PAGE
Figure 1 --	Schematic Diagram of Triode System	28
Figure 2 --	Schematic Diagram of Diode Sputtering Module	29
Figure 3 --	Magnetic Field Profiles of Electromagnet Used in Sputtering	30
Figure 4 --	Ultrahigh Vacuum Facility (Ultek UHV)	31
Figure 5 --	Laboratory Unit for Initial RF Sputtering Work	32
Figure 6 --	Interferometer Pattern of a Step in Deposited Thin Film Dielectric	33
Figure 7 --	Surface of Sputtered Alumina on Experimental Capacitors	34
Figure 8 --	Surface of Sputtered Dielectric on Shorted Capacitor	35
Figure 9 --	Healed Pinhole in Al-Al_2O_3 Capacitor	36
Figure 10--	Multilayer Al-SiO_2 Capacitor with Aluminum Contacts	37
Figure 11--	Multilayer Ta-Al_2O_3 Capacitor with Gold Interconnects	38
Figure 12--	Equivalent Electrical Circuit of a Capacitor	39
Figure 13--	Typical Effect of Frequency on Dissipation Factor of Solid Dielectric Capacitors at Room Temperature	40
Figure 14--	Typical Effect of the Change in Capacitance with Frequency of a Solid Dielectric Capacitor	41
Figure 15--	High Temperature Test Unit	42
Figure 16--	High Temperature Test Unit for Electrical Measurements of Capacitors	43
Figure 17--	Block Diagram of Breakdown Voltage Apparatus	44
Figure 18--	Breakdown Voltage of Al_2O_3 and SiO_2 as a Function of Temperature	45
Figure 19--	The Effect of Frequency and Temperature on Capacitance of Series B-7 Thin Film Capacitors	46

LIST OF FIGURES (continued)

		PAGE
Figure 20 --	The Effect Of Frequency And Temperature On Dissipation Factor of Series B-7 Thin Film Capacitors	47
Figure 21 --	The Effect Of Frequency And Temperature On The Dissipation Factor Of Fused Quartz	48
Figure 22 --	The Effect Of Frequency And Temperature On Capacitance Of Series AC Thin Film Capacitors	49
Figure 23 --	The Effect Of Frequency On Dissipation Factor Of Series AC Thin Film Capacitors	50
Figure 24 --	The Effect Of Temperature On The Dissipation Factor Of Al_2O_3 At A Frequency Of One kHz	51
Figure 25 --	Effect Of Frequency And Temperature On Capacitance Of Series C-4 Thin Film Capacitor	52
Figure 26 --	Effect Of Frequency And Temperature On Capacitance Of Series C-4 Thin Film Capacitor	53
Figure 27 --	Effect Of Frequency And Temperature On Dissipation Factor Of Series C-4 Thin Films	54
Figure 28 --	Effect Of Frequency And Temperature On Capacitance Of Series E Thin Film Capacitor	55
Figure 29 --	Effect Of Frequency And Temperature On Capacitance Of Series E Thin Film Capacitor	56
Figure 30 --	Effect Of Frequency And Temperature On The Dissipation Factor Of Series E Thin Film Capacitor	57
Figure 31 --	The Effect Of Frequency And Temperature On Capacitance Of Series I-2 Thin Film Capacitor	58
Figure 32 --	Effect Of Frequency And Temperature On Capacitance Of Series I-2 Thin Film Capacitor	59
Figure 33 --	Effect Of Frequency And Temperature On Dissipation Factor Of Series I-2 Thin Film Capacitor	60
Figure 34 --	Effect Of Frequency And Temperature On Capacitance Of Series V-1 Thin Film Capacitor	61
Figure 35 --	Effect Of Frequency And Temperature On Capacitance Of Series V-1 Thin Film Capacitor	62

LIST OF FIGURES (continued)

	PAGE
Figure 36 -- Effect Of Frequency And Temperature On Dissipation Factor Of Series V-1 Thin Film Capacitor	63
Figure 37 -- Effect Of Frequency And Temperature On Capacitance Of Series AG Thin Film Capacitors	64
Figure 38 -- Effect Of Frequency And Temperature On Capacitance Of Series AG Thin Film Capacitors	65
Figure 39 -- The Effect Of Temperature And Frequency On Dissipation Factor	66
Figure 40 -- Volume Resistivity Versus Temperature At One kHz Frequency	67
Figure 41 -- The Effect Of Temperature and Frequency On Volume Resistivity	68
Figure 42 -- The Effect Of Temperature On D.C. Resistance	69
Figure 43 -- The Effect Of Temperature On The C (One kHz) x R (D.C.) Product	70
Figure 44 -- The Effect Of Temperature On The Dielectric Constant Of Bulk SiO_2 And Al_2O_3 (Frequency - One kHz)	71
Figure 45 -- The Effect Of Temperature On The Bulk Dissipation Factor Of Al_2O_3 And SiO_2 (Frequency - One kHz)	72
Figure 46 -- The Effect Of Temperature On Dissipation Factor Of Various Capacitor Systems (Frequency - One kHz)	73

RESEARCH INTO THE FEASIBILITY OF THIN METAL AND OXIDE FILM CAPACITORS (U)

by

M. E. Browning
G. V. Jorgenson, and
W. H. Graves

NORTH STAR RESEARCH AND DEVELOPMENT INSTITUTE

SUMMARY

Low energy rf sputtering and vacuum evaporation were used to investigate the feasibility of producing thin metal- and oxide-film capacitors. Dielectric material systems selected for the study included SiO_2 and Al_2O_3, and aluminum and tantalum were examined for the electrodes.

A configuration was established for planar thin film capacitors and various materials systems and deposition procedures were investigated.

SiO_2 and Al_2O_3 capacitors were found to operate effectively at temperatures as high as 300°C, and, in several systems, did not change electrical properties appreciably at temperatures as high as 500°C. The changes that did occur at 500°C were always reversible. Three model capacitors were prepared with interconnected layers having a cumulative volume exceeding 0.5 cubic centimeter of material.

The electrical test characteristics of thin-film SiO_2 capacitors were excellent from -60° to above 300°C, for frequency ranges from 200 to 100,000 hertz. These capacitors demonstrated the feasibility of making planar capacitors that at 300°C had energy densities of 25 joule per kg and dissipation factors of 3×10^{-3}.

INTRODUCTION

In present-day thin film microcircuitry applications, capacitors operate with very low power dissipation. Conventionally, the capacitors do not require high breakdown strengths and do not need to handle high power. In most situations, the problem is reduced to one of employing a capacitor with sufficiently high capacitance and insulation resistance for its application. The dielectric constant for the usual dielectrics lies between 3 and 10. Within this range of dielectric constants, reduction of the thickness of the dielectric is the only means of obtaining higher capacitance per volume. A capacitor fabricated from a material with a dielectric constant of 10 and a thickness of 500 angstroms would have a capacitance of 0.17 microfarads per cm^2. The fabrication of capacitors with dielectrics as thin as 500 Å is difficult because discontinuities and voids are more prevalent, and because insulation resistance and breakdown voltage -- both dependent on film thickness -- suffer as films become thinner. With a uniform film of 2000 Å, the insulation resistance can approach 10^{15} ohm-cm, and up to 30 volts dc can be maintained without breakdown.

Techniques used to date to prepare thin film capacitors employ vacuum evaporation of metals, with subsequent anodic treatment to form the dielectric oxide, or reactive sputtering, where the dielectric is developed by sputtering metal in an oxygen-rich plasma. The technique of low energy radio frequency (rf) sputtering is attractive because of excellence in the control of stoichiometry and film thickness. The technique also yields high-film density and permits a high degree of freedom from pinholes. Improved adherence is also obtained. One reason for improved adherence is that particles arrive at the substrate at much higher velocities than they do, for example, in vacuum evaporation. Thin film inorganic capacitors that can withstand environments up to 500°C and that have higher energy storage capability per unit volume than do presently available inorganic capacitors are of particular interest to the National Aeronautics and Space Administration for applications near energy converters, especially near nuclear reactors.

EXPERIMENTAL PROCEDURE

The four elements of the program to explore the feasibility of preparing thin film capacitors with high capacitance per unit volume and operable up to 500°C are: (1) materials selection, (2) deposition process studies, (3) capacitor development, and (4) testing. High temperature dielectrics, primarily oxides, were reviewed during a screening study. Table 1 lists a number of high temperature compounds of interest for thin film dielectrics.

TABLE 1

CANDIDATE THIN FILM DIELECTRIC MATERIALS AND SPECIFIC PROPERTIES

Compound	Relative Dielectric Constant	Coefficient of Expansion (x 10^{-6}/°C)	Room Temperature Resistivity (ohm-cm)	Dissipation Factor @1 kHz and 25°C
SiO_2 (fused)	3.78	0.55	10^{19}	.0007
SiO	6-7		5 x 10^{6} - 10^{9}	
Al_2O_3	10	9.5	10^{14}	.0014
Si_3N_4	12.7-13.5 Bulk 6.5 Sputtered	2.76	4.1 x 10^{16} ~2 x 10^{13}*	<0.0001 .009
Ta_2O_5	25	1.2		.005
TiO_2	100	9.1	10^{14}-10^{25}	.02-.6
$BaTiO_3$	1000	12.2	3 x 10^{14} 3 x 10^{4}*	

*At 500°C

Material Selection

Screening Studies

Screening studies indicated that both SiO_2 and Al_2O_3 were excellent dielectric materials for preliminary sputtering activities because of their stability at high temperatures and their basic properties (chmical inertness, etc.). Other materials displayed varying

degrees of promise as high temperature dielectric materials, but in most cases, the deposition procedure required extensive refinement, the compatibility with electrode material was a problem, or the electrical properties were lacking in some respect.

Silicon monoxide, frequently studied for integrated circuit and microcircuitry applications[1,2,3], did not have the desired high temperature properties. Moreover, the dielectric constant for thin film SiO decreases as the frequency increases[4]. Some work on Ta_2O_5 films, prepared for experimental capacitors by reactive sputtering, revealed that breakdown voltages were low and that the dielectric constant increases with temperature[5]. Other investigators[6] have observed an instability in both the current-voltage relationship and the capacitance-voltage behavior in reactively sputtered thin films of Ta_2O_5 at temperatures between 25° and 150°C. High temperature nitrides, such as Si_3N_4, were excluded from more detailed examination during screening studies because they offered no real advantage over Al_2O_3 with respect to the electrical properties. Thin films of Si_3N_4 have been prepared by rf and dc reactive sputtering; surface roughness problems were more prevalent in films produced by the dc technique[7]. Barium titanate films have a variety of dielectric constants when flash evaporated[8,9], all very low when compared to the constant of the single crystal material. The properties of rf sputtered barium titanate films vary somewhat depending on substrate temperatures used during deposition[10].

TiO_2 possesses an attractive dielectric constant (100), but recent work indicates that the deposition rates are somewhat lower than for other dielectrics[11]. Reactive cathodic sputtering has been used successfully with improved deposition rates for the preparation of thin TiO_2 layers[12]. Other deposition methods (e.g. chemical vapor deposition[13] and ion beam deposition[14]) also appear promising, but electrical properties appear to vary significantly, depending on operating conditions and substrates used.

Although TiO_2 and $BaTiO_3$ have desirably high dielectric constants, longer lead times required to establish optimum sputtering conditions suggested that the capacitor feasibility trials could be conducted more expediently with SiO_2 and Al_2O_3.

Previous work had shown the feasibility of using reactive sputtering techniques[15] to produce continuous films of SiO_2. The application of rf sputtering techniques, as opposed to reactive sputtering, had been established for quartz several years ago[16,17]. Preliminary trials revealed that SiO_2 could be sputtered effectively, and initial capacitor studies were made using this material.

Prototype Trials

A number of experimental capacitors, 0.635 cm in diameter, were planned as an initial activity. These prototypes were prepared by depositing SiO_2 films on chromium plated steel substrates, followed by depositing aluminum for the other electrode. A typical example of the capacitance for eight capacitors produced on a SiO_2 film, 1.325 microns thick, was 1319 picofarads $\pm$ 3.5 percent. The breakdown voltage of this group was determined to be approximately 70 volts, with a dielectric strength of 2.3×10^6 V per cm. Data obtained indicated that the high dielectric constant of 6.3 may have resulted from an error in film thickness measurements.

Larger capacitors, 2.22 cm diameter, were prepared to assist in examining deposition conditions. Electrical properties were studied for capacitors of various dielectric film thicknesses. Representative of capacitance values obtained was the 0.0145 μf recorded for a 1.05-micron-thick SiO_2 film.

The capacitance of these SiO_2 capacitors is generally within 2.5 percent at all frequencies from 100 Hz to 100 kHz and from room temperature up to about 300°C. Above 300°C, the capacitance rises rapidly with temperature at frequencies below 10 kHz.

For the initial Al_2O_3 dielectric capacitors, fabricated with aluminum electrodes and employing a dielectric layer 3000 Å thick, the results were somewhat different. The capacitance values increased from slightly over 3000 pf to approximately 11,000 pf with a temperature change from ambient to near 500°C. The capacitance-versus-temperature curve was relatively flat between room temperature and 230°C; above that temperature the curve rose rather steeply. Initial trials conducted under various operating conditions revealed some pinhole problems and indicated that more process standardization was needed for the dielectric and electrode deposition. Each was examined separately before further device fabrication was attempted.

Deposition Process Studies

Two deposition processes, vacuum evaporation and sputtering, were investigated for fabricating the thin film capacitors. Vacuum evaporation of metals is well-known and has been described in detail by several authors[18,19]. However, sputtering is not as well-known, and is described briefly below.

Sputtering is generally classified as that deposition process whereby atoms are ejected from a surface as a result of ion bombardment of that surface and are subsequently collected on a substrate. The bombarded surface, or source material, is usually referred to as the sputtering target, and the surface on which the film is deposited is the substrate.

There are several types of sputtering processes, but in this program two types were utilized: dc triode sputtering and rf diode sputtering. The dc triode arrangement, shown in Figure 1, has a thermionic cathode (electron source) and an anode toward which the electrons are accelerated. The process employs a vacuum system, evacuated and then backfilled with argon to about 1 micron pressure. When a potential is applied between anode and cathode, energetic electrons strike argon atoms and cause ionization. The resultant

large number of Ar^+ ions and electrons form an argon plasma. This plasma usually fills the chamber, but can be confined magnetically to increase its density. A metal target is placed in the plasma as the third electrode. When a negative potential is applied to this target, the target is bombarded by the positive argon ions. For example, if the target is made 1000 volts negative with respect to the plasma, it will be bombarded by 1000 eV argon ions. This results in ejection of target material, which is subsequently collected on a substrate. This technique was used in the project for depositing electrode materials such as stainless steel, copper, titanium, and tantalum. Gold and aluminum were more conveniently deposited by vacuum evaporation.

Insulating materials cannot be deposited in the same way. It is not possible to impress a negative dc voltage on an insulator. In attempting to do so, the surface becomes charged positively from the bombarding ions because the charge cannot be conducted away. Ultimately, the surface becomes positively charged to a point where bombardment stops. To circumvent this condition, rf voltage is applied to a metal plate placed in contact with the insulator target and shielded from the plasma. Because the target is an insulator, the net current flowing to it is zero. However, because of the large difference between electron mobility and ion mobility, the surface becomes increasingly negatively charged during the first few cycles. It thus becomes biased to the point where the electron and ion currents are equal in any one cycle. The electrical voltage pattern of such a system is shown below.

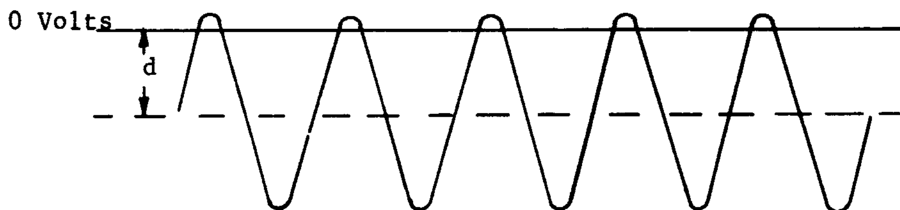

The displacement (d) of the 0 volt line is self-bias. The rf voltage has to become only slightly positive to gain its electrons. When it becomes negative, it is bombarded by an equal number of ions, which cause sputtering.

North Star used the rf diode arrangement shown in Figure 2. The target is attached to the high voltage electrode and the substrate table is the other electrode. In this system, the rf not only provides sputtering voltage but also causes plasma excitation. The frequency used in this system is 13.56 MHz, a frequency within the band alloted to industry, science, and medicine.

A more nearly complete discussion on rf voltage interactions with a plasma is given by H. S. Butler[20].

Initial Deposition Studies

Early laboratory work employed a McDowell 1.5 KW-2VFD rf power supply for sputtering the candidate dielectrics. An 18 x 10-inch bell jar system was set up with anode and cathode for dc plasma excitation. An rf feed-through (Consolidated Vacuum Corporation) was installed for applying the rf sputtering voltage to the target. A Kovar-glass target was fabricated for the rf sputtering trials.

In the first rf sputtering runs, the magnet for constricting the plasma, and thus increasing plasma density, acted as an antenna, picking up the rf signal and feeding it back to the magnet's power supply. A capacitor was added to the magnet circuit to filter out the rf signal.

It was found that rf sputtering of metal targets worked very well. However, when the metal was covered with an insulator, the best conditions were obtained when the tuning capacitor in the rf supply was at one extreme of the tuning range. A "matching-box" (inductor and variable capacitors) was added between the rf supply and the rf feed-through to extend the tuning range so that the load could be impedance-matched to the output of the rf supply. All conceivable combinations of the rf supply frequency (2-40 MHz) and output tuning, as well as "matching-box" tuning, were examined. Deposition rates for insulating materials with this arrangement were found to be too low (< 10 Å/min) to be useful in producing experimental capacitors.

Problems in system design and component construction plagued initial studies. Typical of difficulties experienced in these trials were the power tube failures in the McDowell generator. During one rf sputtering run, the rf power tube failed as a result of a power induced crack in the glass envelope. The tube was replaced and two sputtering runs later, the problems recurred. The McDowell rf power supply was returned to the manufacturer, where it was found to produce sufficient parasitic oscillations to crack the tubes. Several components were replaced, including the tuning capacitor for load matching purposes. These modifications improved the operation significantly. A new R. D. Mathis rf sputtering module, placed in service at that time, performed sufficiently well to warrant its use on all subsequent rf sputtering tasks.

Magnetic fields were used in both the dc triode system and the R. D. Mathis system to increase plasma density. Studies showed that the use of magnets significantly increased the deposition rates. A 750-turn magnet was used to produce an axial magnetic field (parallel to the vertical axis through the target and the substrate table) and the magnet was normally operated at 2 amperes.

Magnetic field strength measurements were made to relate field strength to plasma density. The magnetic field strength and profile for the 750-turn electromagnet with 2 amperes dc applied is shown in Figure 3, in which the magnet position is shown at the bottom. Curve "a" was plotted from data obtained starting at one edge of the magnet, while curves "b" and "c" were made at distances of 6 and 12 inches, respectively, from the same edge. A transverse magnetic field probe (Bell model 120) was used, and all measurements were made of the field strength parallel to the axis of the magnet. In the case of the rf system, the magnet is approximately centered on the target-substrate space. In the case of the dc triode system, the anode-to-cathode spacing is approximately one foot and the level of the magnet is near the anode as shown previously in Figure 1.

Studies in Ultrahigh Vacuum

A number of sputtering runs were made in the Ultek ultrahigh vacuum system. A ½-inch thick stainless steel plate was placed on the system in place of the 19-inch bell jar. A six-inch diameter Pyrex cylinder was positioned over a 4½-inch hole in the plate, and the R. D. Mathis target assembly and the tuning unit was placed on top of the glass cylinder. Typically, the system pressure before admitting argon varied between 7×10^{-9} and 2×10^{-8} Torr as read on the ion gage. The corresponding pressures in the ion pump were about 1×10^{-8} to 3×10^{-8} Torr. Figure 4 shows the arrangement used.

There were minor problems experienced in obtaining good capacitors in the ultrahigh vacuum system because of faulty adhesion and some shorting. This may have been caused by depositing SiO_2 on uncooled substrates. The thermal expansion mismatch between the SiO_2 and the electrode material may have promoted crazing when the coupled materials were cooled to room temperature. The substrate table used in these trials had no provisions for water cooling. An alternate table with cooling capabilities was considered but found unusable because it had a lubricated movable feed-through, not suitable for ultrahigh vacuum use.

A typical capacitor prepared in the ultrahigh vacuum system was 0.635 cm in diameter with 1.34μ thick SiO_2 film deposited on a chromium-plated steel substrate. Aluminum top electrodes completed the device. Capacitance values were near 1,000 pf with parallel resistance values of 2.5×10^{-8} ohms. A value of ~ 5 was calculated for the dielectric constant.

It appears that differences between capacitors produced in high vacuum and those prepared in ultrahigh vacuum systems will probably become apparent only in long-term exposure to elevated temperatures. In that case, the additional trapped background gas in the films prepared in the high vacuum system will probably have some affect on the film characteristics.

Capacitor Development

Electrodes

All of the aluminum electrodes were vacuum evaporated by conventional techniques, using tungsten wire filaments. Auxiliary substrates were utilized for producing steps so film thickness could be measured on an interferometer. Tantalum electrodes were produced by dc sputtering. Gold interconnections were produced by vacuum evaporation.

Dielectrics

The following is typical of the procedures used for depositing a dielectric film by sputtering in the R. D. Mathis rf system:

> The target was clamped to the water-cooled rf electrode, using a thin coating of vacuum grease for better heat transfer. The Al_2O_3 target (Cerac, Inc.) was four inches in diameter and ½ inch thick. The SiO_2 target (General Electric, Co. Type 101 clear fused quartz) was five inches in diameter and 1/8 inch thick. The substrate was cleaned by scrubbing with detergent, rinsing with both tap water and deionized water, and drying in a stream of clean dry air. The substrate was placed on the substrate table spaced two inches from the target. After the system was evacuated to the lower 10^{-5} Torr range, it was then back-filled with Ar through the needle leak valve to a pressure of 1 to 2 x 10^{-3} Torr. The magnetic field was introduced by passing a current of two amperes through the 750-turn electromagnet. Cooling water to the rf electrode and the substrate table then had to be turned on. The plasma was ignited by turning on the rf power, the "matching-box" (matching load to the 50 ohm output of transmitter) was tuned for minimum reflected power and the transmitter output

adjusted to give 2,000 volts rf voltage to the target. The system is capable of operating at higher rf voltages, but the higher voltages produce considerably more heat, and better thermal contact would be required both at target and substrate for satisfactory operation.

After sufficient film was deposited, the rf generator and the magnet were turned off. Following this, the vacuum valve was closed, but the Ar leak valve was left open. This allowed the Ar pressure to build up and speeded cooling by transferring heat from hot components to the water-cooled components. After five to ten minutes, the cooling water was turned off, and the system was brought to atmospheric pressure and opened. The initial facility is shown in Figure 5.

Film Thickness Measurements

In all deposition runs, a small auxiliary substrate was placed near the primary substrate to obtain thickness measurements. A thin section of quartz (0.010 in) was on the auxiliary substrate in order to create a physical step from substrate to upper surface of film. This step was measured interferometrically using a Reichert metallographic microscope equipped with a Nomarskii polarization interferometer. The film thickness can be determined by the equation:

$$\Delta h = \left(n + \frac{\Delta d}{d}\right)\left(\frac{\lambda}{2}\right) \qquad (1)$$

where Δh - film thickness

Δd = fringe displacement

λ = wavelength of light

n = an integer

The integer, n, can readily be determined using white light as shown in Figure 6a. It can be seen that the pattern at the step is deflected slightly less than 3 full fringes. Since the deflection is

more than 2 fringes, the integer n is 2. The lines become sharper in monochromatic light (Figure 6b) making measurement of the fractional fringe ($\frac{\Delta d}{d}$) easier. In this case $\frac{\Delta d}{d}$ = 0.824 and λ = 5890 Å. Thus, the film thickness in Figure 6 is 2.824 x 2945 Å - 8317 Å. The precision is approximately ± 50 Å from a single measurement. By knowing the exact deposition time, we can determine deposition rates for various operating conditions. The time is then subsequently controlled to yield the desired film thickness in later runs. In each succeeding experiment, another "step check" is made to determine the thickness and the deposition rate for the film produced.

Examination of Capacitors and Substrates

Several capacitors of Al - Al_2O_3 were subjected to microscopic examination to determine the origin of the pinhole shorts in the capacitors. Figures 7a and 7b show regions of the alumina (9,000 Å thick) over an aluminum thin film in two sets of capacitors. The capacitors formed by the film shown in Figure 7a revealed no shorts. All of the capacitors formed on the film shown in Figure 7b were shorted and could not be healed by applying a high current to burn out the shorts.

The dark grey defects in the film shown in Figure 8 are asperities in the alumina substrate that extend above the glazed surface. During alumina deposition, they are not coated well and result in shorts. These substrate asperities were also observed in uncoated, glazed substrates. Figure 8 represents a particularly poor substrate in terms of asperity density. Most of the substrates had only a few or no asperities.

Figure 9 shows a minor pinhole that has been healed by "burn-out" of the thin aluminum strand that had permeated the pore. Current flows through the short when dc power is applied to the capacitor. When the current rises sufficiently, the aluminum in the short evaporates, eliminating the short. This does not work with higher melting electrode materials.

Most of the pinholes in films such as these are believed caused by dust[21,22]. In our work, the longer the highly cleaned substrates were exposed to laboratory atmosphere before deposition, the more pinholes were formed in the films produced. Dust can be effectively eliminated and the capacitor yield optimized by performing the entire operation in a clean room and in a system equipped so that vacuum does not have to be broken between deposited layers of a stacked capacitor.

In general, dielectric film thicknesses used for experimental capacitors varied from about 3000 to 14,000 Å for SiO_2 and from about 3000 to 20,000 Å for Al_2O_3. In the Al_2O_3 capacitor systems some films were prepared to thicknesses of 75,000 Å. The lower film thicknesses were preferred for ease of deposition.

Multilayered Capacitor Preparation

Multilayered Al - SiO_2 capacitors were produced on glazed Al_2O_3 substrates. The four SiO_2 dielectric layers deposited to make up a typical test capacitor averaged approximately 3,400 Å and were separated by vacuum-evaporated aluminum electrodes. Figure 10 shows the configuration with the deposited aluminum contacts at the corners. The center disk is the electrode stack. Tabs of odd-numbered electrodes make contact at one corner, and of even-numbered electrodes at the other corner. One fourth-inch diameter contacts (Al) were added to make testing easier.

A more complex Ta - Al_2O_3 multilayer system was designed and procedures were established for producing interconnecting layers by using a mask during deposition. A typical capacitor of this series is shown in Figure 11. It is composed of several Al_2O_3 dielectric layers and alternating Ta electrodes. This series demonstrated the feasibility of depositing capacitors of large volume, the volume of each capacitor being more than 0.17 cm^3.

Electrical Tests

Electrical tests were conducted to determine capacitance, dissipation factor and breakdown voltage as functions of frequency and temperature for the various capacitors constructed.

The two-terminal equivalent electrical circuit of a capacitor may be represented by a series resistance (R) and inductance (L) connected to a parallel combination of capacitance (C) and conductance (G) as shown in Figure 12. The series resistance and inductance represent the equivalent circuit of the capacitor's connecting leads and electrodes. The capacitance exists between the capacitor plate electrodes and the conductance represents the losses of the solid dielectric between the capacitor plates.

At low frequencies, the effects of the series resistance and inductance are negligible and the capacitor acts as a pure capacitance in parallel with a conductance. As the frequency is increased, the inductance becomes an important consideration because a condition of resonance occurs between (L) and (C). For frequencies below resonance, the inductance partially neutralizes the effect of the capacitance, resulting in an effective terminal capacitance given approximately by the following equation (Equations given in this section are derived in the Appendix):

$$C_t = \frac{C}{1-\omega^2 LC} \qquad (2)$$

The dissipation factor for a capacitor is defined as the ratio of the energy dissipated to the energy stored. In terms of the equivalent circuit of Figure 12 the dissipation factor is given by:

$$D = \frac{R + \dfrac{G}{\omega^2 C^2 + G^2}}{\omega L - \dfrac{\omega C}{\omega^2 C^2 + G^2}} \qquad (3)$$

At low frequencies, and for the case of a reasonably good capacitor; e.g.

$$L = 0$$
$$G^2 \ll \omega^2 C^2$$

the total dissipation factor is (4)

$$D = \omega CR + \frac{G}{\omega C}$$

For a solid dielectric capacitor, the dominant component of the conductance is the loss in the dielectric. The loss varies with frequency. The dissipation factor is directly proportional to the energy dissipated and is the sum of the three principal components.

1. A constant dissipation factor caused by residual polarization.
2. Interfacial polarization loss.
3. Series resistance in the leads and capacitor plates.

The total dissipation factor has a minimum value at the frequency that varies inversely with capacitance. The minimum usually occurs between 1 kHz and 1 MHz.

A typical result for the variation of dissipation factor with frequency at room temperature for a solid dielectric capacitor is shown in Figure 13. The residual polarization results in a constant dissipation factor and is shown by the horizontal dotted line. The loss produced by interfacial polarization is represented by the dotted line that slants downward to the right. Ohmic losses in the leads and plates are shown by the dotted line slanting upward to the right. The series resistance (R) is not usually significant at low frequencies. As the frequency is increased, the skin effect becomes significant, the resistance increases, and is a function of the square root of the frequency. This resistance relationship may be expressed as $R\sqrt{f}$, where R is the resistance at 1 MHz and (f) is the frequency in megahertz. The total dissipation factor at high frequencies is then:

$$D = \frac{G}{\omega C} + R_1 \sqrt{f} \omega C \quad (5)$$

At low frequencies, the only losses that are important are represented by the parallel conductance (G).

In addition to the high frequency effect of the inductance of capacitor leads and electrodes, an effect occurs at low frequencies that causes a capacitance change with frequency. The capacitance increases at low frequencies because of dielectric absorption resulting from interfacial polarization in the dielectric. A typical result of capacitance change with frequency is shown in Figure 14. The dotted line slanting downward to the right represents the change in the dielectric constant of the dielectric resultant of interfacial polarization. The line slanting upward to the right is the effective change in capacitance caused by the series inductance.

Table 2 lists the capacitor types on which extensive electrical tests have been performed. The results of the tests are reported in the following sections.

Test Equipment

Electrical tests have been made using a General Radio Type 1615A capacitance bridge and sample holder. A special high temperature holding device was fabricated for making elevated-temperature electrical measurements. A high-temperature furnace was modified to allow direct connection of the specimen holder to the capacitance bridge. This laboratory facility is shown in Figure 15. The high temperature test cell was fabricated from stainless steel, Inconel, and glass-bonded mica. Platinum contact wires and a tip were used to prevent oxidation difficulties. Arrangement of the components is shown in Figure 16.

Test Results

The early measurements of breakdown voltage were made by manually contacting the capacitor electrode with a probe connected

TABLE 2

TYPICAL CAPACITOR SYSTEMS REPRESENTING RANGE OF DIELECTRIC THICKNESSES EXAMINED

Series	Dielectric Material	Average Dielectric Thickness (angstroms)	Capacitor Diameter (inches)	Electrodes		Substrate	Characteristic Dielectric Strength (V/cm)
				Top	Bottom		
B	SiO_2	4,500	0.250	Al	Cr	Chromium Plated Steel	1.1×10^6
C	SiO_2	9,000	0.250	Al	Cr	Chromium Plated Steel	4.7×10^6
E	SiO_2	10,250	0.875	Al	Cr	Chromium Plated Steel	1.0×10^6
I	Al_2O_3	3,000	0.250	Al	Al	Al_2O_3	1.3×10^7
V	Al_2O_3	19,500	0.250	Al	Al	Al_2O_3	9.2×10^5
AC	Al_2O_3	38,000	0.250	Ta	Ta	Tantalum	1.2×10^6
AG	Al_2O_3	75,000	0.250	Ta	Ta	Tantalum	-

to a power supply. The power supply was current-limited, so the voltage was increased until the ammeter registered current flow. The accuracy of these measurements was doubtful because contact pressure would vary considerably and the pressure might be enough to damage certain capacitors.

The measurement apparatus was then set up as shown in Figure 17. This utilizes the same sample holder used for capacitance and dissipation factor measurements, and the contact pressure is the same on all samples. All capacitor series that were measured both ways gave higher breakdown voltages in the sample holder. There were no capacitors remaining in series B and E for additional measurements; consequently, dielectric strengths for B and E are probably higher than shown in Table 2.

Some preliminary measurements of dielectric strength versus temperature were made on both SiO_2 and Al_2O_3 films. The results of these measurements are shown in Figure 18. The spread in points on the SiO_2 curve probably is not related to temperature, but rather indicates a variation from one capacitor to another on the same substrate. At this time it has not been determined whether the same is true for Al_2O_3. At 300°C, the dielectric held 510 volts, the limit of the power supply.

Figures 19 and 20 illustrate results obtained on a capacitor of 0.250 inches diameter with the dielectric of SiO_2 on a chromium-plated steel substrate. The thickness of the dielectric in this group, denoted Experimental Capacitor Series B, is 4,500 Å. The top electrode is formed of vacuum evaporated aluminum. In Figure 19 the capacitance variation is shown as a function of frequency and temperature. At frequencies above 10 kHz, the capacitance varies less than two percent from approximately room temperature to 390°C. Figure 20 shows the variation of dissipation factor with frequency and temperature. The results at 138°C are approximately as would be expected for SiO_2 dielectric material. As the temperature is increased, the minimum value of the dissipation factor moves toward a higher frequency,

indicating an increase in dielectric losses because of interfacial polarization. Published values[23] of dissipation factors as a function of frequency and temperature for fused quartz are plotted in Figure 21.

Figures 22 and 23 show results obtained on a capacitor system that has been fabricated with a dielectric of Al_2O_3. The capacitor, 0.250 inch in diameter, is on a tantalum substrate with a tantalum top electrode. The dielectric thickness for this series (AC) is 38,000 Å. Figure 22 shows the effect of frequency and temperature on the capacitance. As found in capacitors with SiO_2 dielectric, the capacitance has only a small variation over the temperature range for frequencies from 10 kHz to above 100 kHz. In Figure 23, the dissipation factor is shown as a function of frequency for a temperature of $22^{o}C$. For this particular capacitor system, the dissipation factor is higher than for the SiO_2 system illustrated in Figure 20. Published values[24] of the bulk dissipation factor of Al_2O_3 as a function of temperature at a frequency of 1 kHz are plotted in Figure 24.

Figures 25, 26, and 27 show results obtained on a series C capacitor that has an identical configuration to the series B, except that the dielectric of C is thicker. For the series C devices, the capacitor diameter was 0.250 inch, the dielectric was sputtered SiO_2, and a chromium plated steel substrate was used. The series C capacitors were fabricated with a dielectric thickness of 9,000 Å, twice that used for the series B devices.

The effect of frequency and temperature on capacitance is shown in Figures 25 and 26 for temperatures from 22° to $520^{o}C$. At 100 kHz, the capacitance varies about two percent from 22° to $520^{o}C$. Figure 27 shows the effect of frequency and temperature on the dissipation factor.

Series E is another capacitor series similar to B and C. Devices in this series also have SiO_2 dielectric layers with chromium plated steel used as the substrate. The differences are the dielectric thickness and capacitor diameter which are 10,250 Å and 0.875 inch,

respectively. Results of electrical measurements on series E are shown in Figures 28, 29, and 30. The effect of frequency and temperature on capacitance from -60° to $520^{\circ}C$ is shown in Figures 28 and 29. From -60° to $320^{\circ}C$, we noted that the capacitance changed only about 2.3 percent for frequencies from 200 Hz to 100 kHz. Only at a temperature of $520^{\circ}C$, and for frequencies below 100 kHz, does the capacitance depart significantly from the values at lower temperatures.

The dependency of dissipation factor on frequency and temperature for series E is shown in Figure 30. For the lower frequencies and temperatures, the dissipation factor is less than approximately 10×10^{-4}.

Two capacitor series with a dielectric material of Al_2O_3 and aluminum electrodes were subjected to extensive electrical tests. Devices that were examined are the I and V series, which are identical except for the thickness of the dielectric material. Both series were fabricated using Al_2O_3 substrates and have capacitor diameters of 0.250 inch. The series I capacitors have a dielectric thickness of 3,000 Å while the series V have an average thickness of 19,500 Å. Figures 31, 32, and 33 show the pertinent electrical characteristics for temperatures from -57° to $520^{\circ}C$. For temperatures from -57° to approximately $300^{\circ}C$, a greater change in capacitance occurs with Al_2O_3 systems at the low frequencies than does with the SiO_2 dielectric series.

Figures 34, 35, and 36 show results obtained for capacitance studies of the series V devices. The effect of temperature and frequency on capacitance and dissipation factor are shown to be quite similar to that observed in series I devices, except that there is a slight upward shift in the series I dissipation factor at 100 kHz for temperatures of $135^{\circ}C$ and below. As in the series I, the change in capacitance as a function of temperature is greater than that shown by the series B, C, or E.

To examine the effect of tantalum electrodes on Al_2O_3 dielectrics, two series of devices, AC and AG , were fabricated identically except for dielectric thickness. Series AC devices, test data shown previously in Figures 22 and 23, revealed lower capacitance values than those found for the series AG devices. Curves for series AG devices, presented as Figures 37, 38, and 39 are similar to those obtained for the companion devices, AC series, with their thinner dielectrics.

Volume resistivity measurements were performed on two capacitor series. The value of the parallel conductance (G) was measured and the volume resistivity computer from

$$\text{Resistivity} = \frac{1}{G} \quad \frac{\text{Area of Capacitor Electrode}}{\text{Dielectric Thickness}} \qquad (6)$$

(ohm-cm)

Figures 40 and 41 show results of measurements for the series E and AG capacitors as a function of temperature and frequency. The series E volume resistivity is shown in Figure 40 for a frequency of 1 kHz. Results for the AG series are shown in Figure 41 for frequencies from 1.0 to 100 kHz. The series E has a dielectric of SiO_2 and the series AG, Al_2O_3. Comparing results at 1 kHz the volume resistivity of the series E is superior by a factor of approximately 100.

The dc resistance as a function of temperature was measured for two capacitor series. Series I represents a single layer capacitor with a dielectric of Al_2O_3. Series AH is a four layer capacitor with a SiO_2 dielectric. Figure 42 shows the test results for both series. Both series have nearly identical dc resistances as a function of temperature.

A quantity that can be used for determining the quality of a capacitor in a filter circuit is the C (1 kHz) x R (dc) product. The series AH has a capacitance of approximately 11,000 picofarads for temperatures from 22° to over 300°C. Precise capacitance measurements were performed on the series AH for frequencies from 200 Hz to 100 kHz

throughout the temperature range from 22° to 512°C. Results of the capacitance and the dc resistance measurements were used to calculate the C (1 kHz) x R (dc) product which is shown in Figure 43. Results for the series I-2 were obtained from the data given in Figures 31, 32, and 42.

Property Review

Dielectric Strength. Bulk strength for SiO_2 is 1.6 x 10^5 V/cm and for Al_2O_3 it is approximately 8.4 x 10^4 V/cm. The dielectric strengths shown earlier in Table 2 reflect the common increase in dielectric strength for thin films. For Al_2O_3 this trend is already evident at 1 mm where the dielectric strength is 2.8 x 10^5 V/cm. Below about 2000 Å thickness, however, the breakdown strength might decrease due to discrete film defects and interfacial roughness. Dielectric strengths measured in this program were generally in the 10^6 V/cm range and this agrees well with what others have found for thin films of these materials[25].

Capacitance. The variation of capacitance with frequency and temperature is less for the SiO_2 dielectric capacitors than for the Al_2O_3 devices. Table 3 tabulates the percentage capacitance change for SiO_2 and Al_2O_3 capacitor systems for a temperature range from 22° to approximately 300°C at a frequency of 1 kHz. The table shows the small variation in capacitance for SiO_2 systems compared to the large changes experienced by Al_2O_3 dielectrics. The major cause of capacitance change can be attributed to the temperature dependence of the dielectric material. Figure 44 shows values of dielectric constant for SiO_2 and Al_2O_3 measured at a frequency of 1 kHz. The change of dielectric constant for SiO_2 is insignificant for temperatures from 22° to 300°C. Only above 300°C does the dielectric constant increase appreciably. A different situation exists for Al_2O_3. The dielectric constant experiences a significant change with temperature. For the case of the field perpendicular to the optic axis the dielectric constant changes by more than 20 percent for the temperature range from 22° to 300°C.

TABLE 3

CAPACITANCE CHANGE IN SiO_2 AND Al_2O_3
CAPACITOR SYSTEMS AT 1 kHz

Series	Temperature Range	Percent Variation
C (SiO_2)	22° to 317°C	1
B (SiO_2)	22° to 300°C	1.2
E (SiO_2)	22° to 320°C	1.25
AH (SiO_2)	22° to 314°C	0.33
I (Al_2O_3)	22° to 295°C	59
V (Al_2O_3)	22° to 318°C	26
AG (Al_2O_3)	22° to 332°C	3
AC (Al_2O_3)	22° to 300°C	23

Dissipation Factor. A preliminary analysis of the effect of temperature on dissipation factor of SiO_2 and Al_2O_3 capacitor systems can be made by examining measurement data. Figure 45 shows the dissipation factor at temperatures of 22° and approximately 300°C for selected capacitors. Data is for measurements at 1 kHz. The SiO_2 capacitors have a dissipation factor an order of magnitude less than the Al_2O_3 devices over the temperature range considered. Figure 46 illustrates bulk dissipation factors for Al_2O_3 and SiO_2 for a frequency of 1 kHz. The spread in dissipation factor noted for the measured capacitors is not evident from Figure 46. The greater dissipation factors of the Al_2O_3 units cannot be attributed to electrode thickness. Further effort will be devoted to this area.

CONCLUSIONS AND RECOMMENDATIONS

Thin film capacitors were prepared by low energy rf sputtering and vacuum evaporation using dielectric materials of SiO_2 and Al_2O_3. Results of electrical tests indicated that both dielectric materials can be employed effectively in capacitors operating at temperatures as high as 300°C, and in several cases to temperatures as high as 500°C, with little change in electrical properties.

Specifically, laboratory work demonstrated the feasibility of making planar thin-film SiO_2 capacitors with excellent electrical characteristics from -60° to above 300°C for frequency ranges from 200 to 100,000 hertz.

From the results of this initial study, it is recommended that additional research be undertaken to develop dielectric films of primarily SiO_2 or Al_2O_3 for high temperature capacitors with thicknesses between 2,000 and 5,000 angstroms, with higher thickness uniformity and with higher deposition rates. Other high dielectric constant materials, as well as new techniques for preparing capacitors without breaking vacuum, should be investigated.

REFERENCES

1. Budenstein, P. P., and Hayes, P. J., Appl. Physics, 38, No. 7, 2837 (June 1967).
2. Chaiken, S. W., and St. John, G. A., Electrochem. Tech., 1, 294 (1963).
3. Liben, W., et al, Microelectronic Engineering, 1, Fabrication Technology, Johns Hopkins University (November 1965).
4. Maddocks, F. S., and Thun, R. E., J. Electrochem. Soc., 109,(2), 99-103 (1962).
5. Pavlovic, A. S., J. Chem. Phys [illegible]0, 951-956 (1964).
6. Szedon, J. R., et al, J. Electrochem. Soc., 114, 59C ([illegible]).
7. Hu, S. M., J. Electrochem. Soc., 113,(7), 693 (1966).
8. Brown, V. R., Thirteenth National Vacuum Symposium, San Francisco, 8-5 (1966).
9. Muller, E. K., Nicholson, B. J., and Francombe, M. H., Electrochem. Tech., 1, 158 (May-June 1963).
10. Feuersanger, A. E., et al, J. Electrochem. Soc., 111,(12), 1387 (1964).
11. Terry, L. E., Final Report ECOM-02212-F (U. S. Army Electronics Command) 56 (February 1968).
12. Perny, G., et al, Compt Rend., Ser. C., 263,(4), 265-268 (1966).
13. Feuersanger, A. E., IEEE, Proc., 52, 1463-1465 (December 1964).
14. Chopra, K. L., Rev. Sci. Instrum., 38,(8), 1147-1151 (1967).
15. Valletta, R. M. et al, Electrochem. Tech., 4, 402-406 (1966).
16. Anderson, G. S., Mayer, W. N., and Wehner, G. K., J. Appl. Physics, 33, 2991-2992 (October 1962).
17. Davidse, P. D., and Maissel, L. I., J. Appl. Phys., 37,(2) 574 (February 1966).
18. Holland, L., Vacuum Deposition of Thin Films, Chapman and Hall, Ltd., London (1963).
19. Steinberg, H. A., Handbook of High Vacuum Engineering, Reinhold Publishing Corporation, New York, 274-299 (1963).

20. Butler, H. S., "Plasma Sheath Formation by RF Fields", DDC Report No. AD-260088 (1961).

21. Rol, P. K., et al, Trans. Int'l Vac. Congr., 3rd Stuttgart, 1, 75-82 (1965).

22. Vernickel, H., Z. Naturforsch, 21(8), 1308 (1966).

23. von Hippel, A., Dielectric Materials and Applications, The MIT Press, Cambridge, Massachusetts, 403 (1954).

24. Ibid, 371.

25. Maissel, L. I., Physics of Thin Films, 3, G. Hass and R. Thun, eds., Academic Press, New York, 113 (1966).

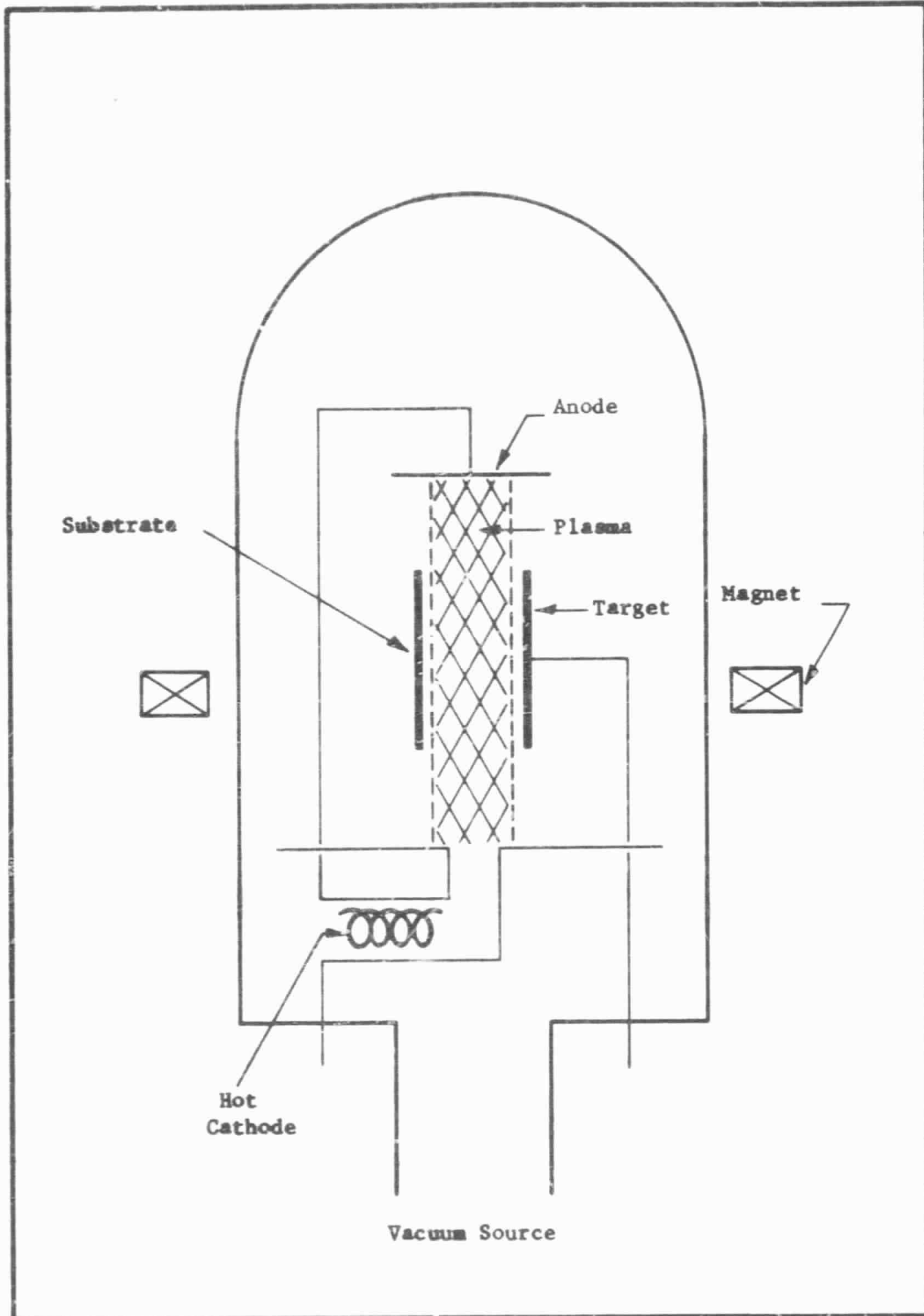

FIGURE 1. SCHEMATIC DIAGRAM OF TRIODE SYSTEM

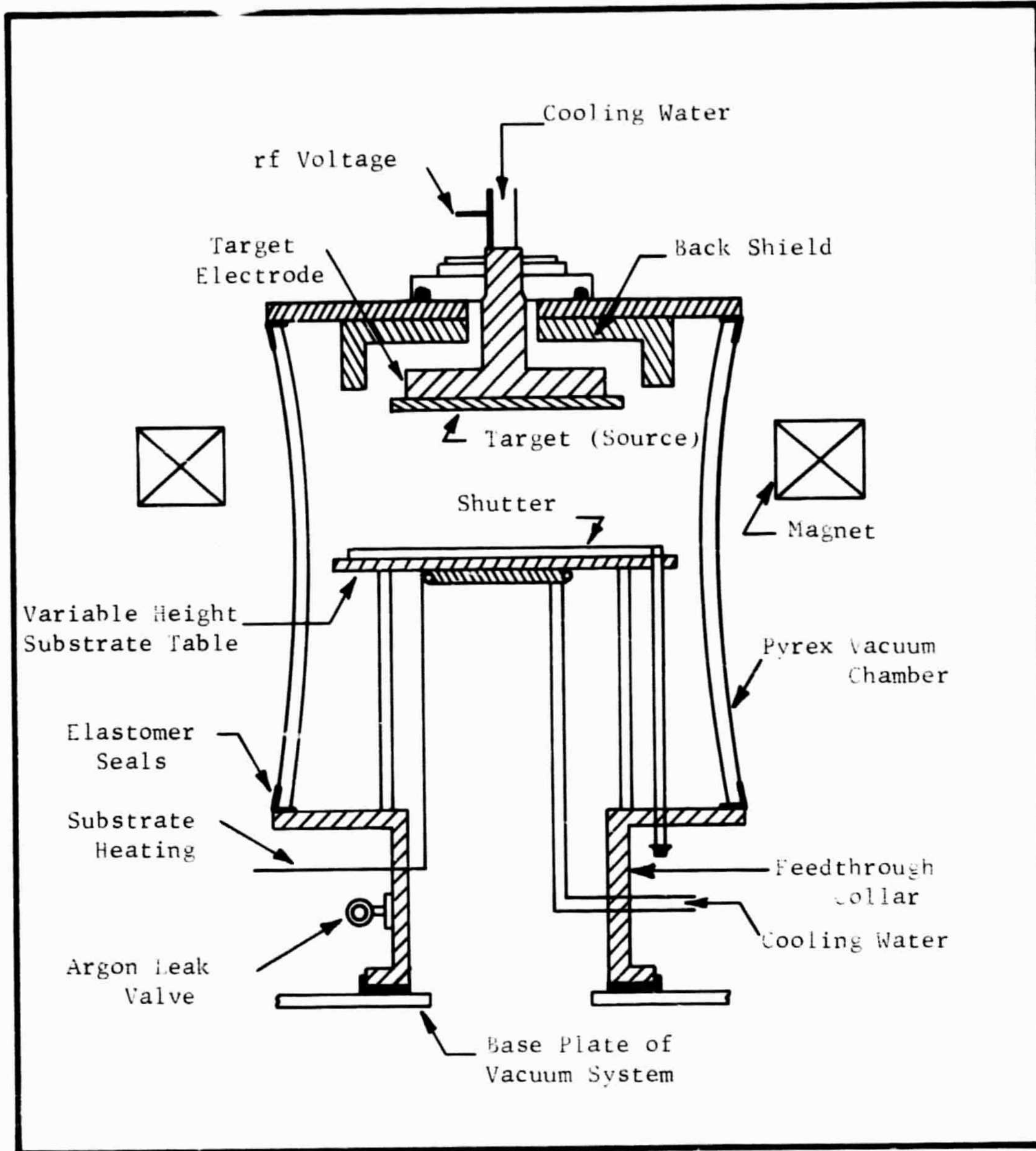

FIGURE 2. SCHEMATIC DIAGRAM OF DIODE SPUTTERING MODULE

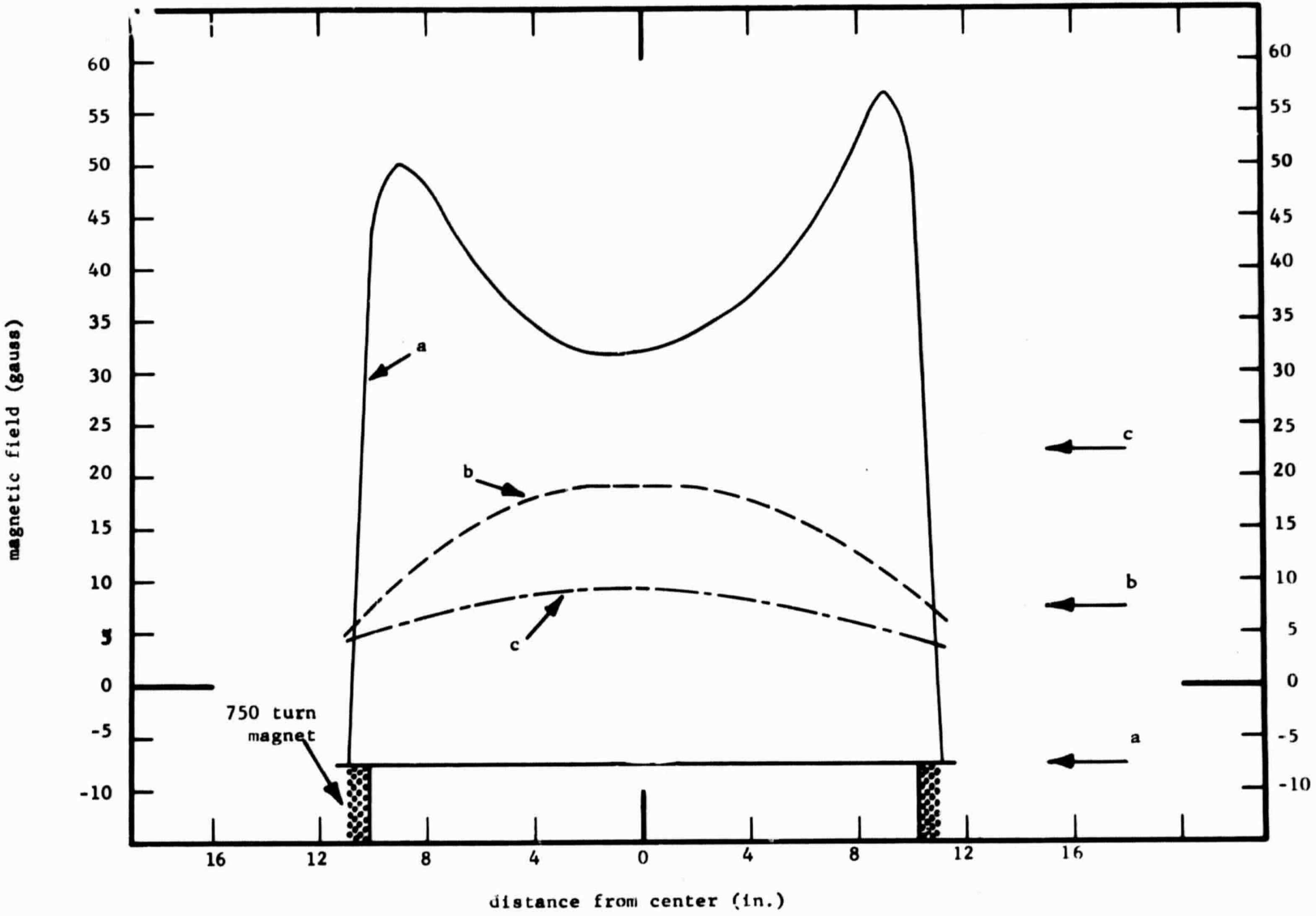

FIGURE 3. MAGNETIC FIELD PROFILES OF ELECTROMAGNET USED IN SPUTTERING

FIGURE 4. ULTRAHIGH VACUUM FACILITY (ULTEK UHV)

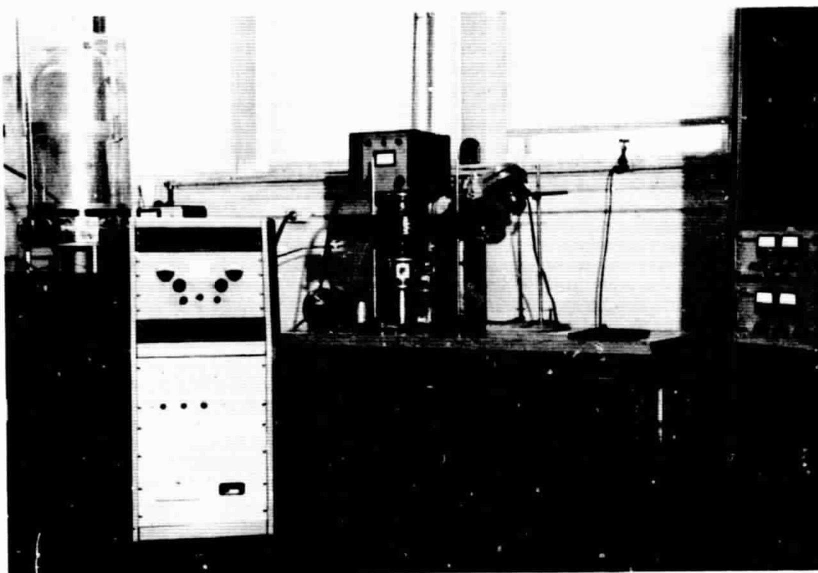

FIGURE 5. LABORATORY UNIT FOR INITIAL RF SPUTTERING WORK

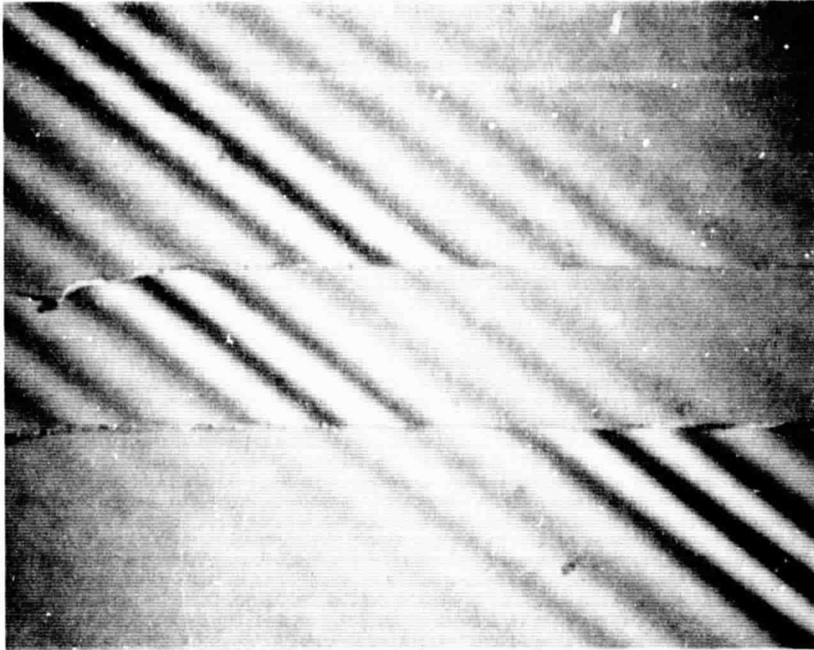

a. Using white light for determination of integer (n)

b. Using monochromatic light

FIGURE 6 INTERFEROMETER PATTERN OF A STEP IN DEPOSITED THIN FILM DIELECTRIC.

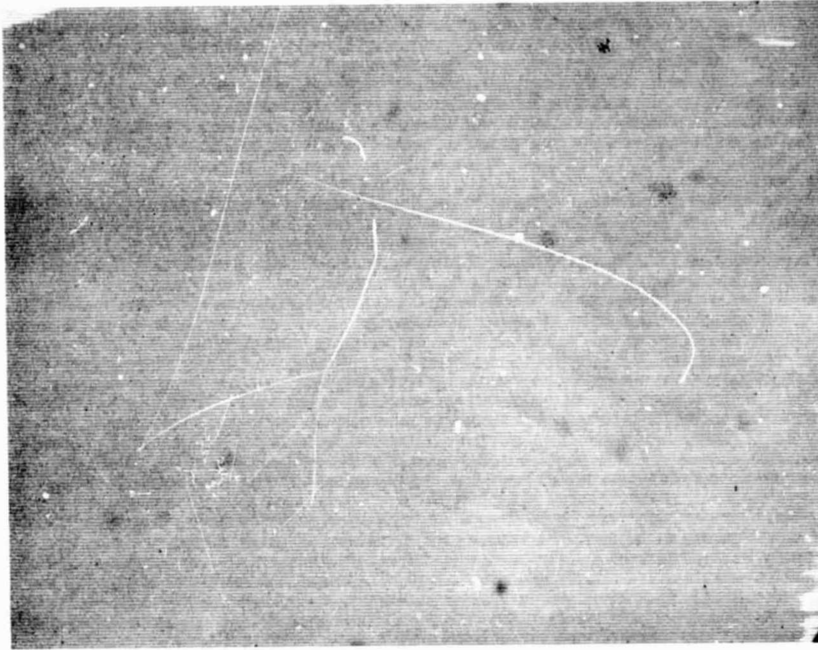

(375X)

a. Unfailed Capacitor (No Shorts)

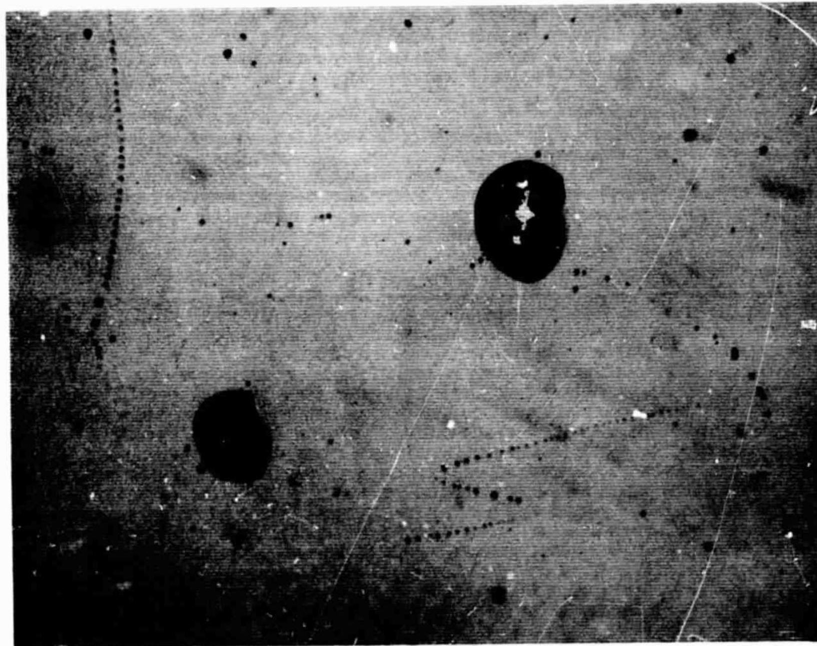

b. Shorted Capacitor (375X)

FIGURE 7. SURFACE OF SPUTTERED ALUMINA ON EXPERIMENTAL CAPACITORS

(375 X)
Substrate: Glazed Alumina
Electrode: Aluminum
Dielectric: Sputtered Alumina
9000 Å Thick

FIGURE 8. SURFACE OF SPUTTERED DIELECTRIC ON SHORTED CAPACITOR

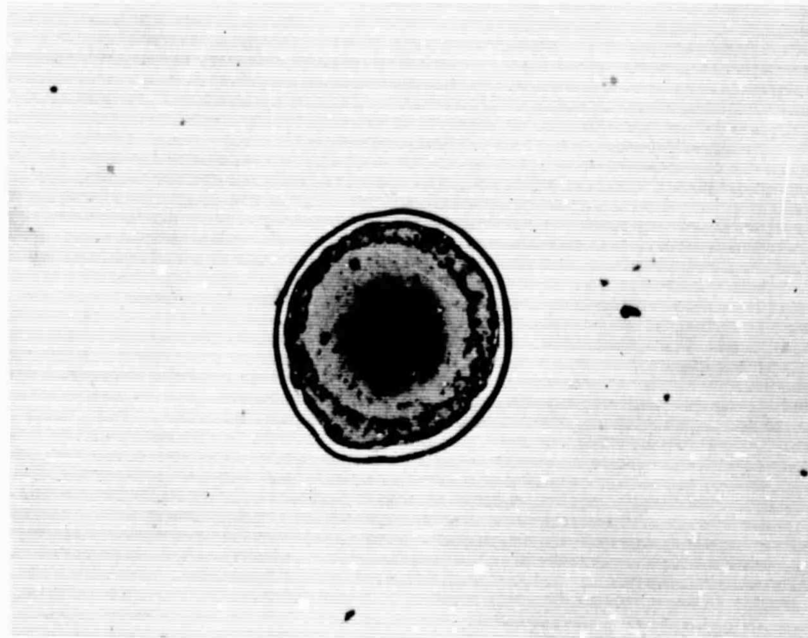

(250 X)

FIGURE 9. HEALED PINHOLE IN Al - Al_2O_3 CAPACITOR

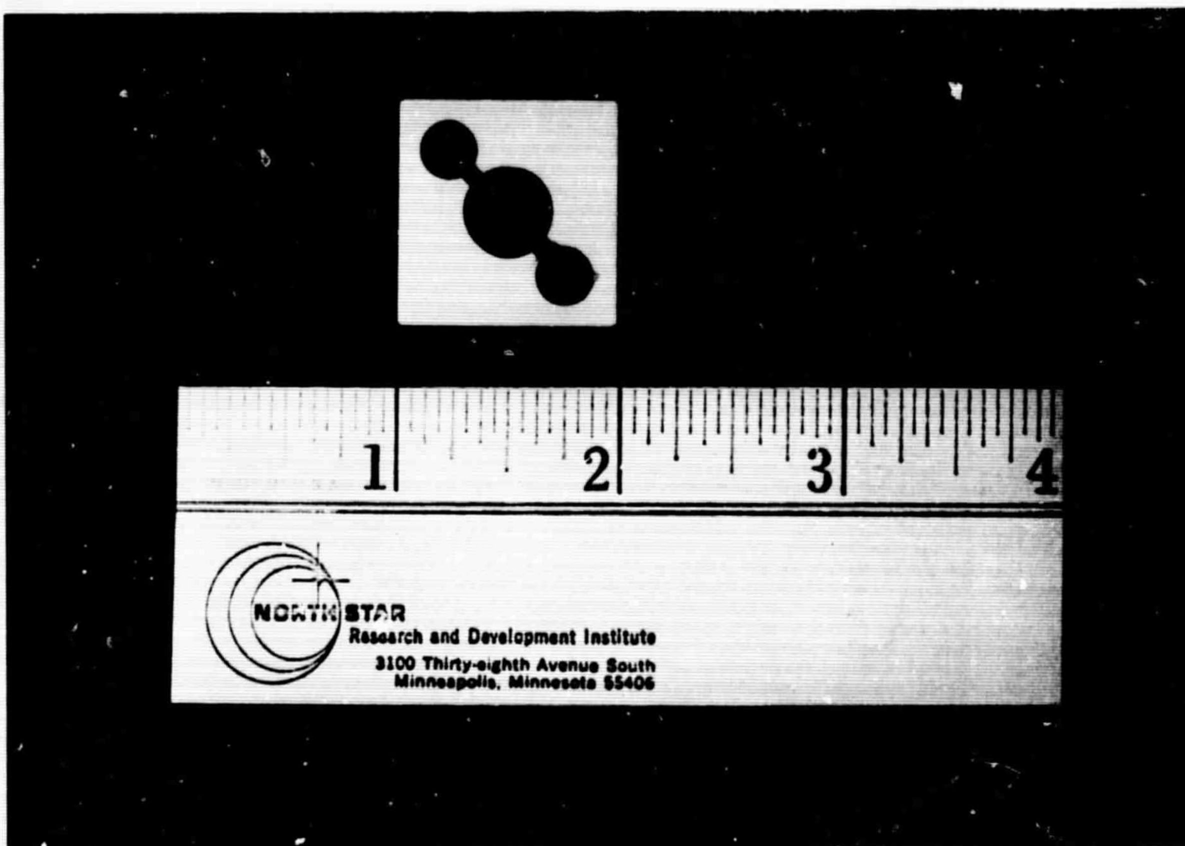

FIGURE 10. MULTILAYER Al - SiO_2 CAPACITOR WITH ALUMINUM CONTACTS

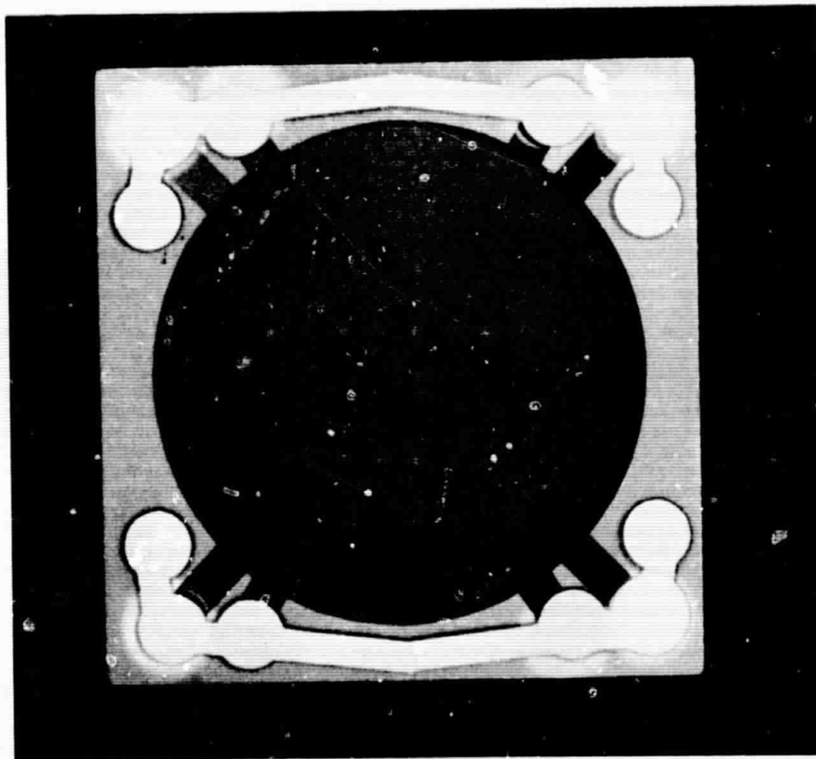

FIGURE 11. MULTILAYER Ta - Al_2O_3 CAPACITOR WITH GOLD INTERCONNECTS

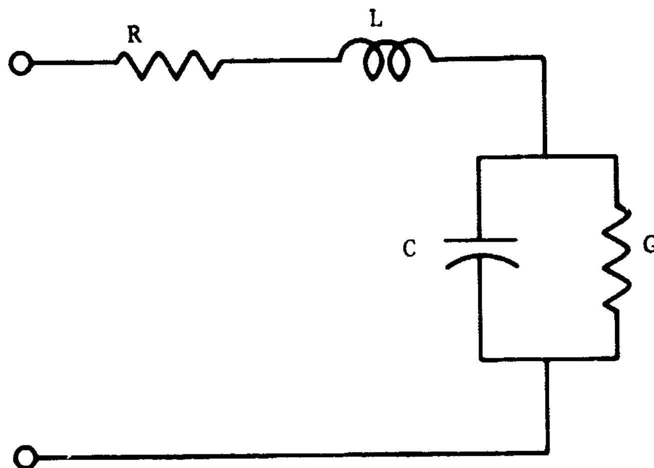

FIGURE 12. EQUIVALENT ELECTRICAL CIRCUIT OF A CAPACITOR

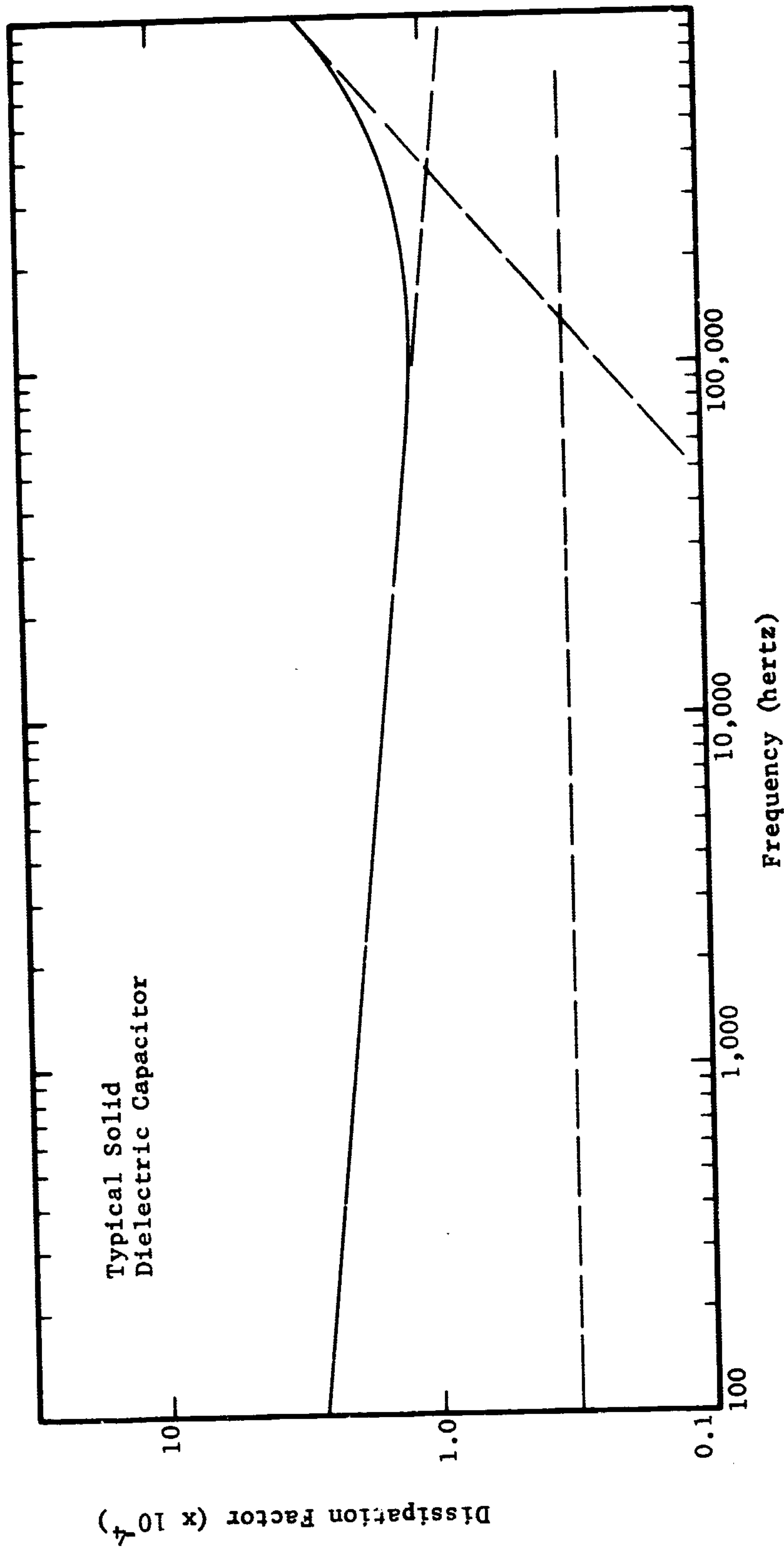

FIGURE 13. TYPICAL EFFECT OF FREQUENCY ON DISSIPATION FACTOR OF SOLID DIELECTRIC CAPACITOR AT ROOM TEMPERATURE

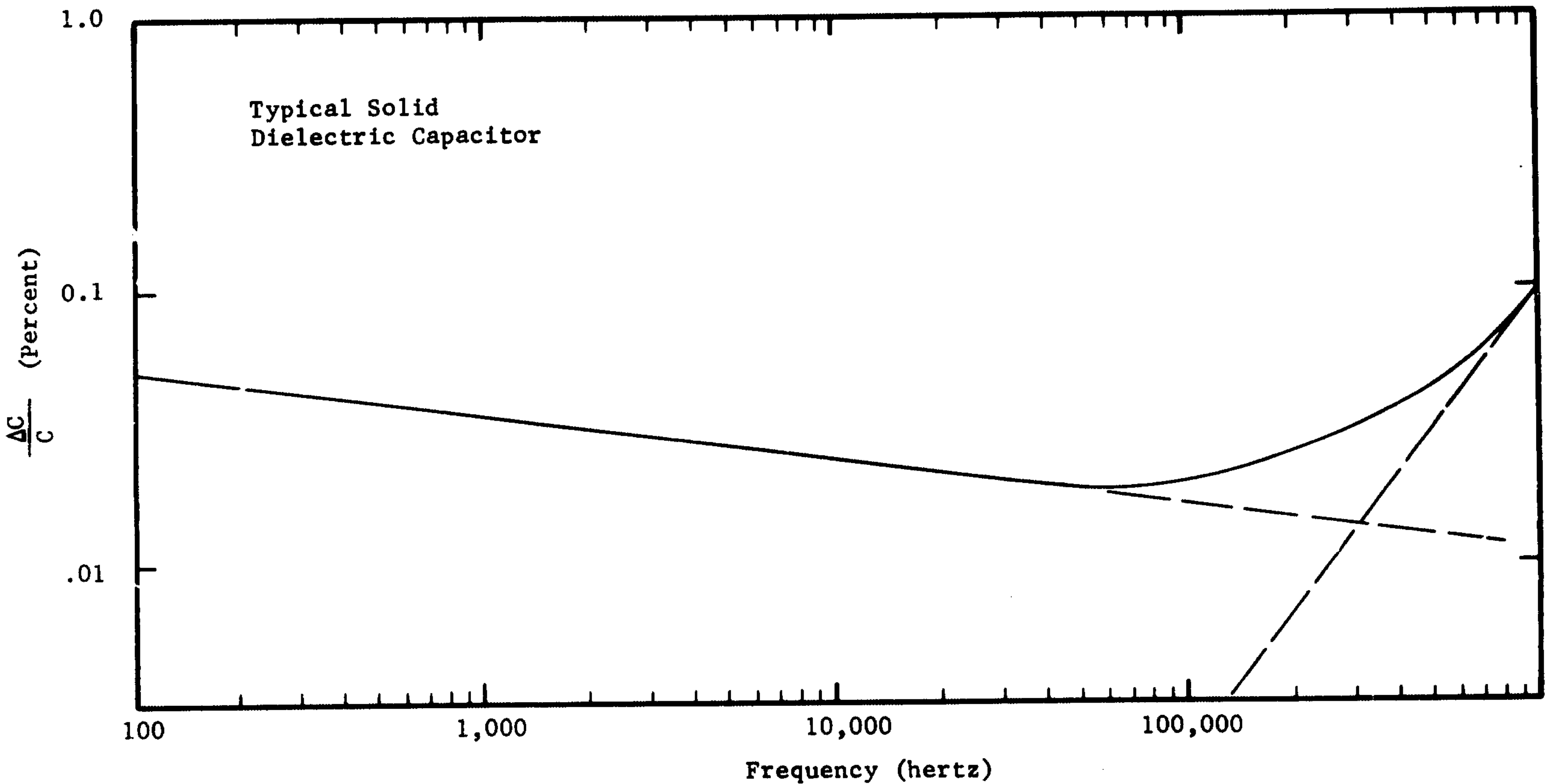

FIGURE 14. TYPICAL EFFECT OF THE CHANGE IN CAPACITANCE WITH FREQUENCY OF A SOLID DIELECTRIC CAPACITOR

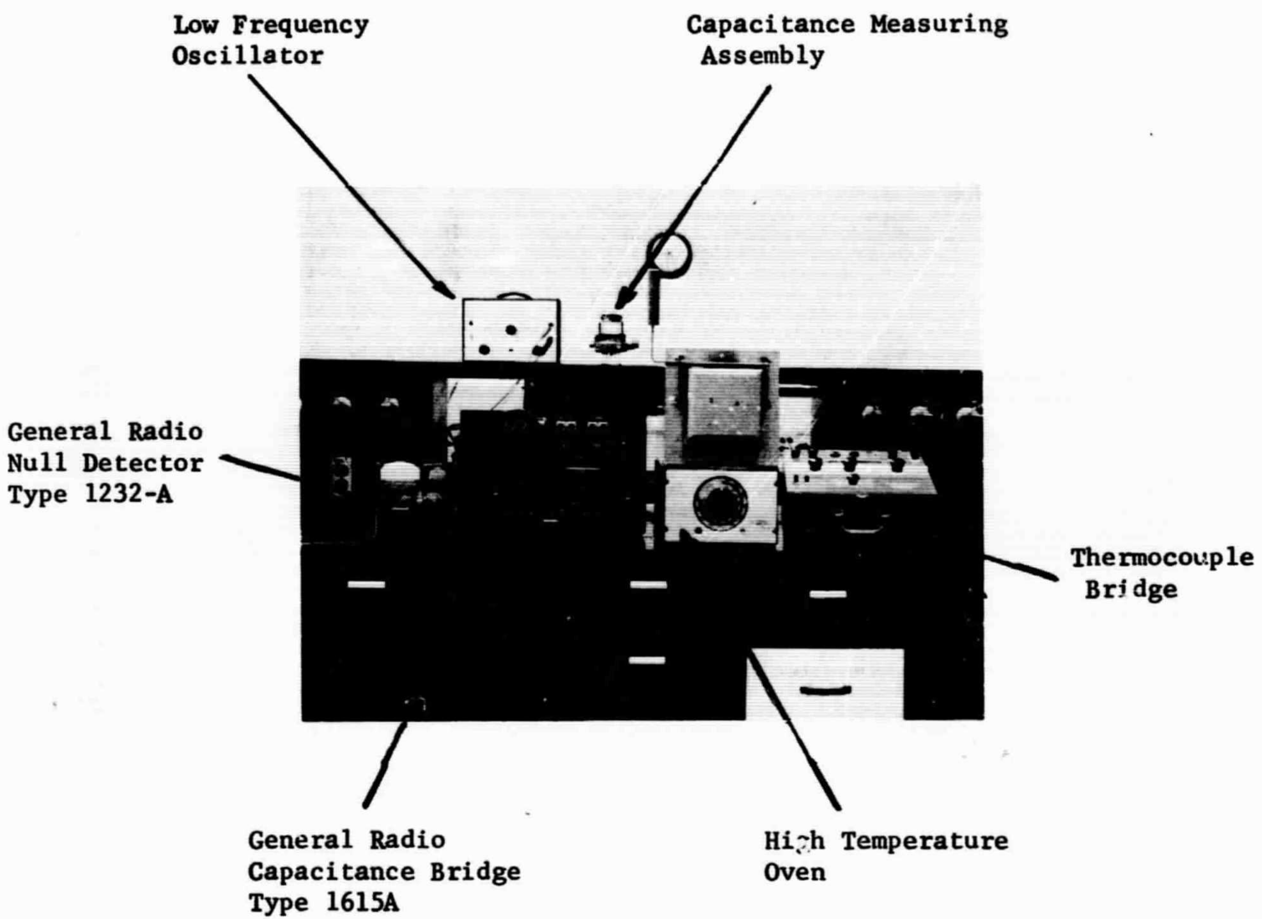

FIGURE 15. HIGH TEMPERATURE TEST UNIT

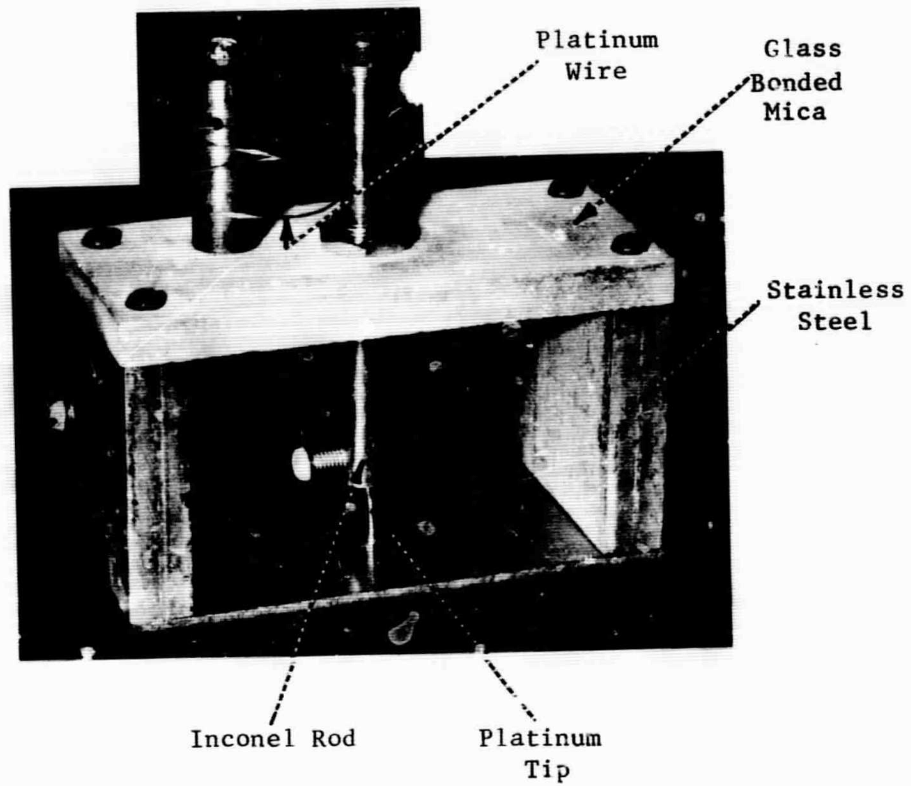

FIGURE 16. HIGH TEMPERATURE TEST UNIT FOR ELECTRICAL MEASUREMENTS OF CAPACITORS

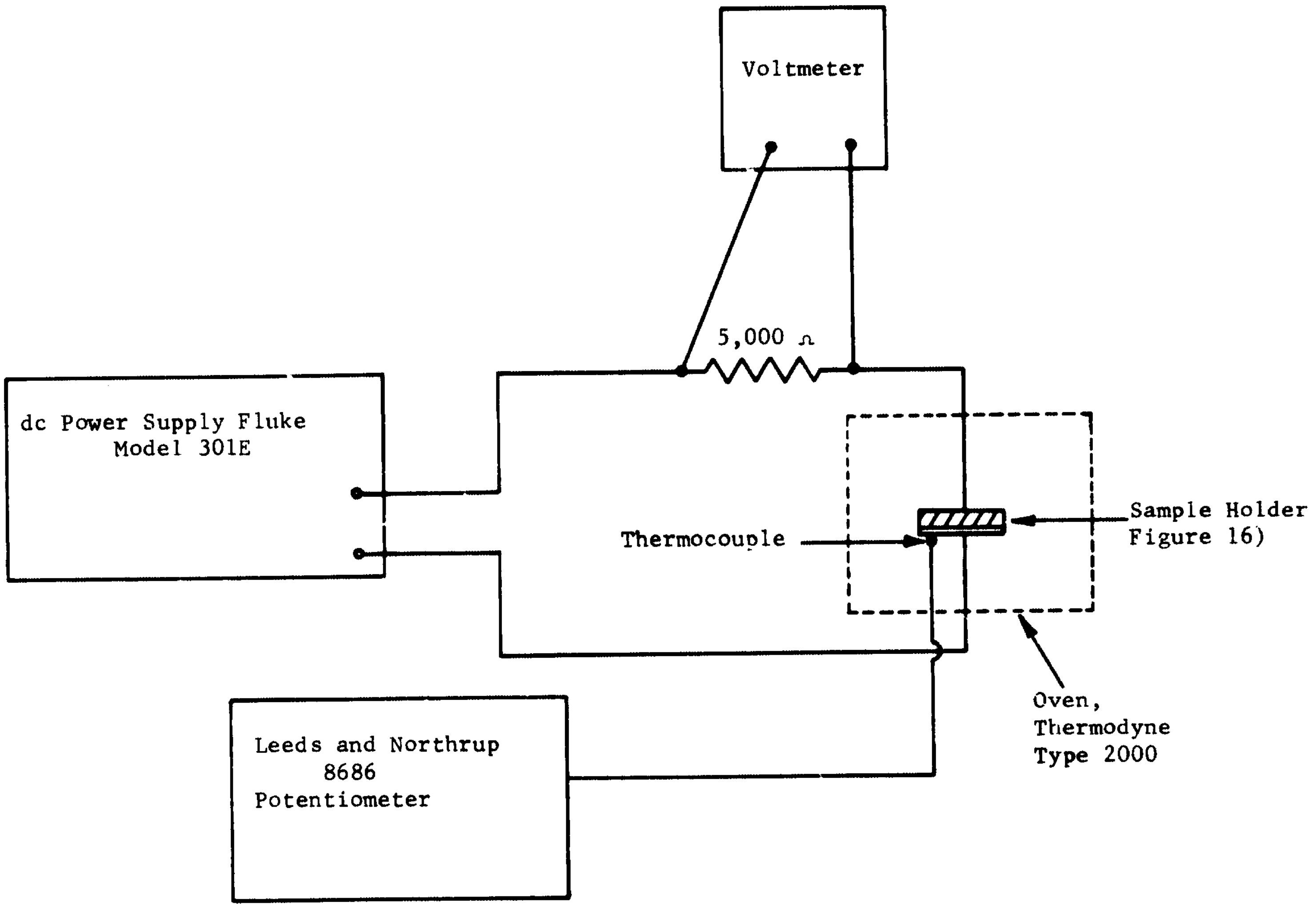

FIGURE 17. BLOCK DIAGRAM OF BREAKDOWN VOLTAGE APPARATUS

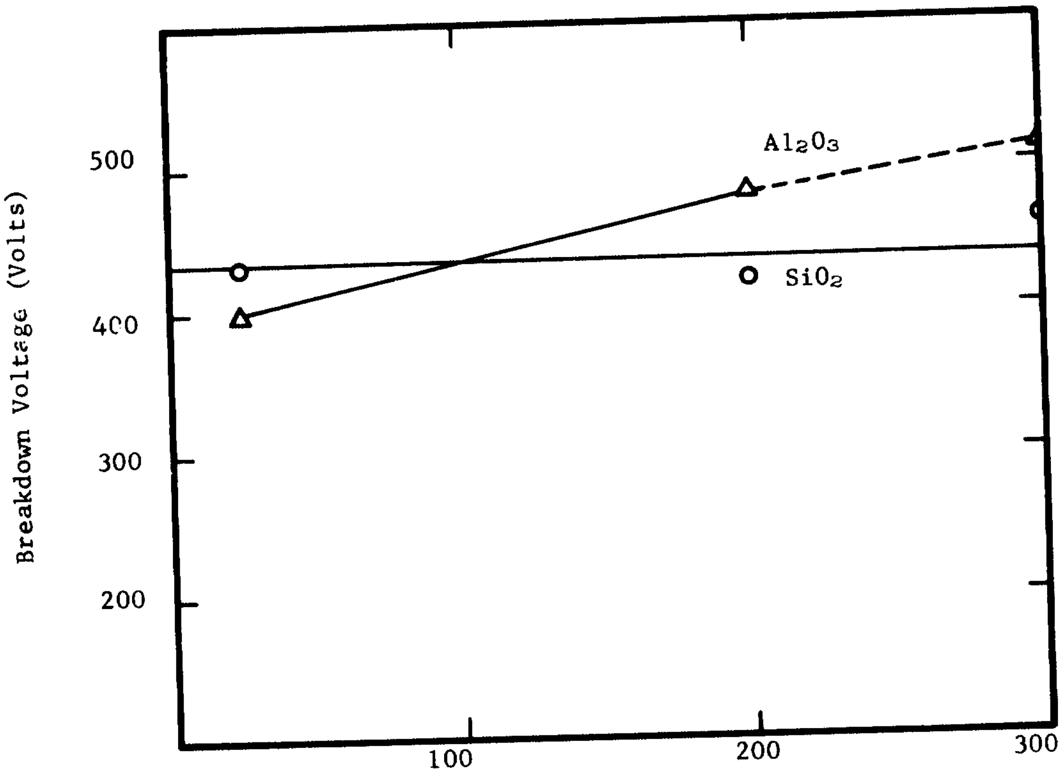

FIGURE 18. BREAKDOWN VOLTAGE OF Al_2O_3 AND SiO_2 AS A FUNCTION OF TEMPERATURE

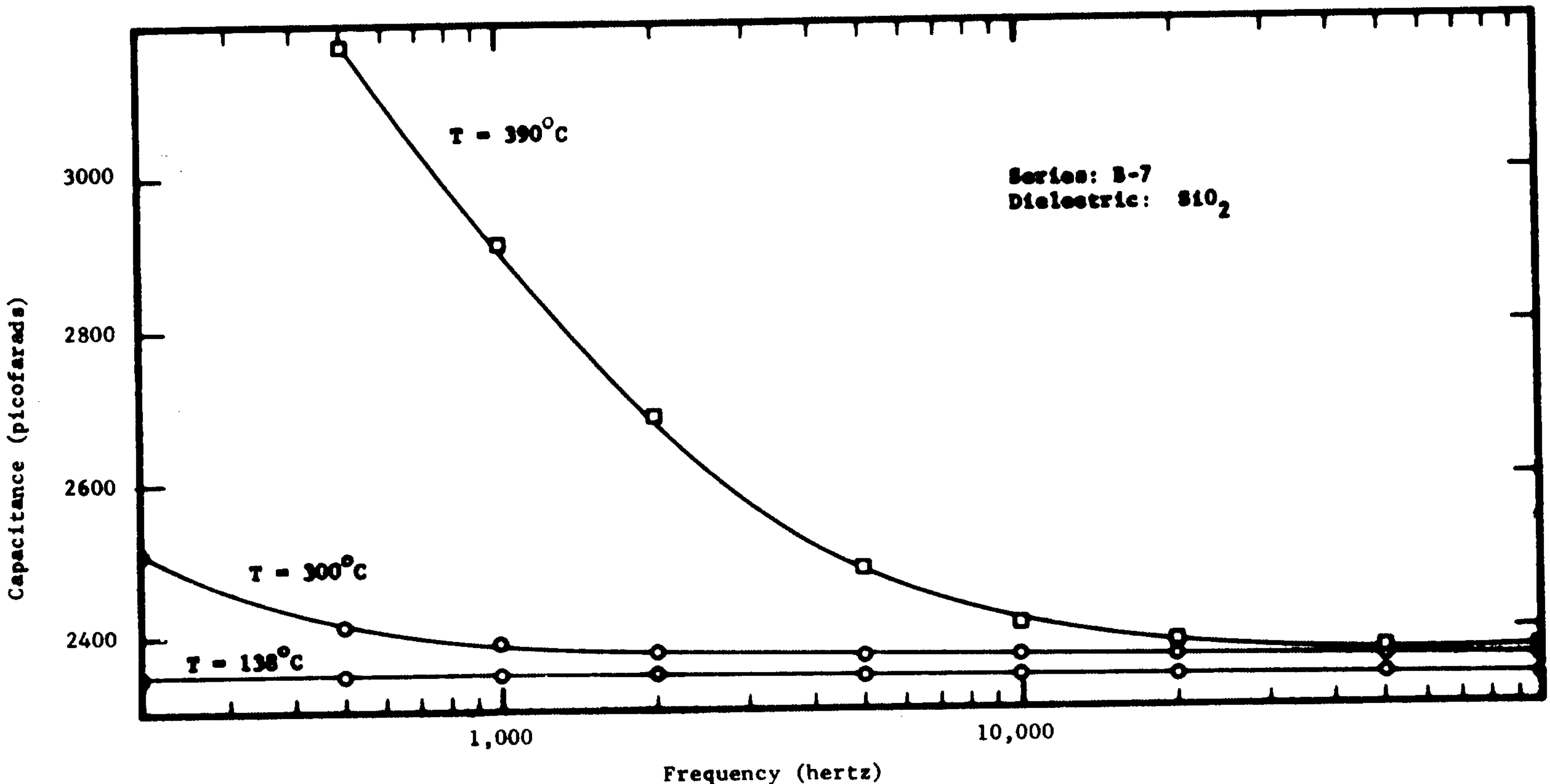

FIGURE 19. THE EFFECT OF FREQUENCY AND TEMPERATURE ON CAPACITANCE OF SERIES B-7 THIN FILM CAPACITORS

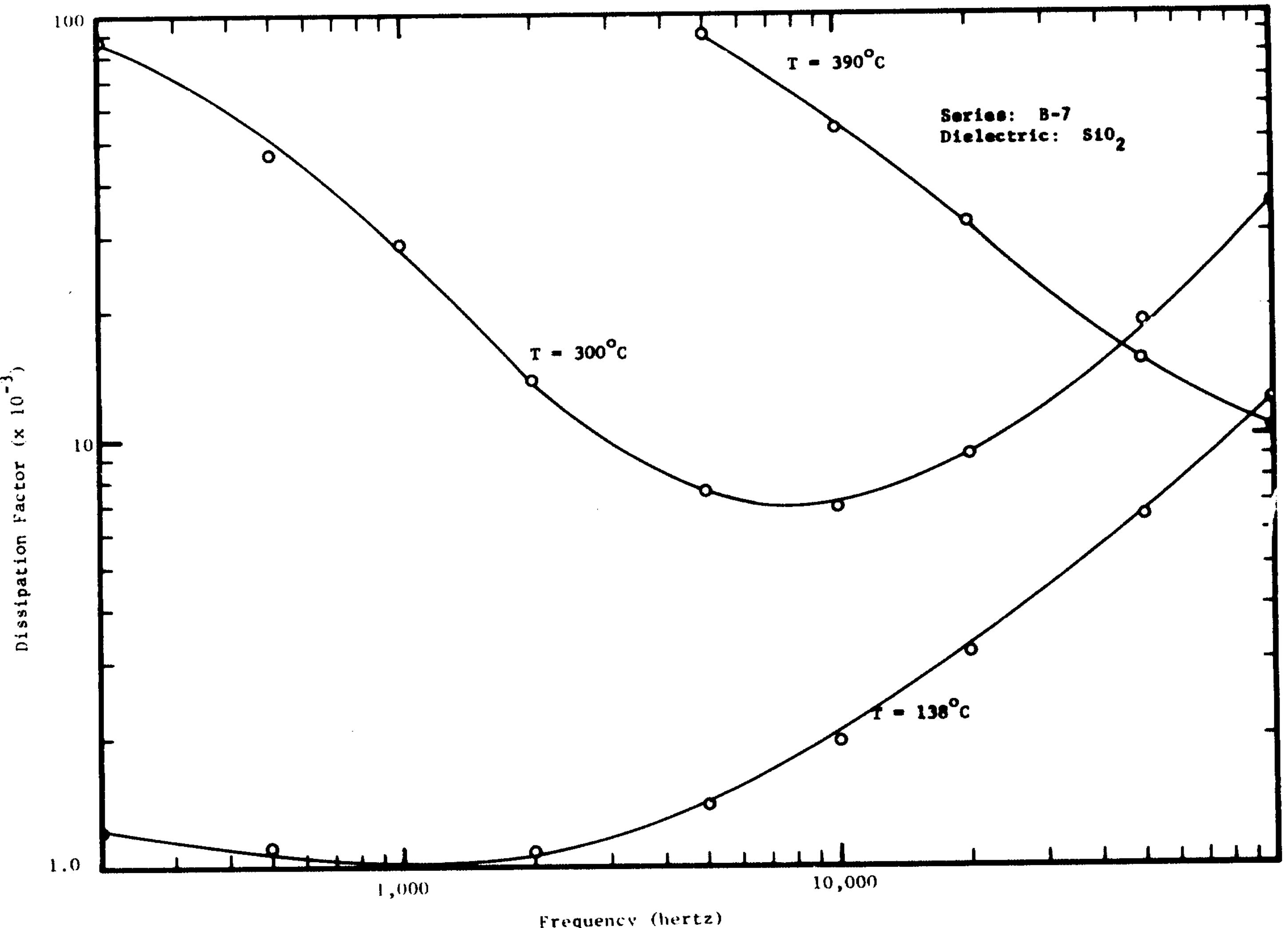

FIGURE 20. EFFECT OF FREQUENCY AND TEMPERATURE ON DISSIPATION FACTOR OF SERIES B-7 THIN FILM CAPACITORS

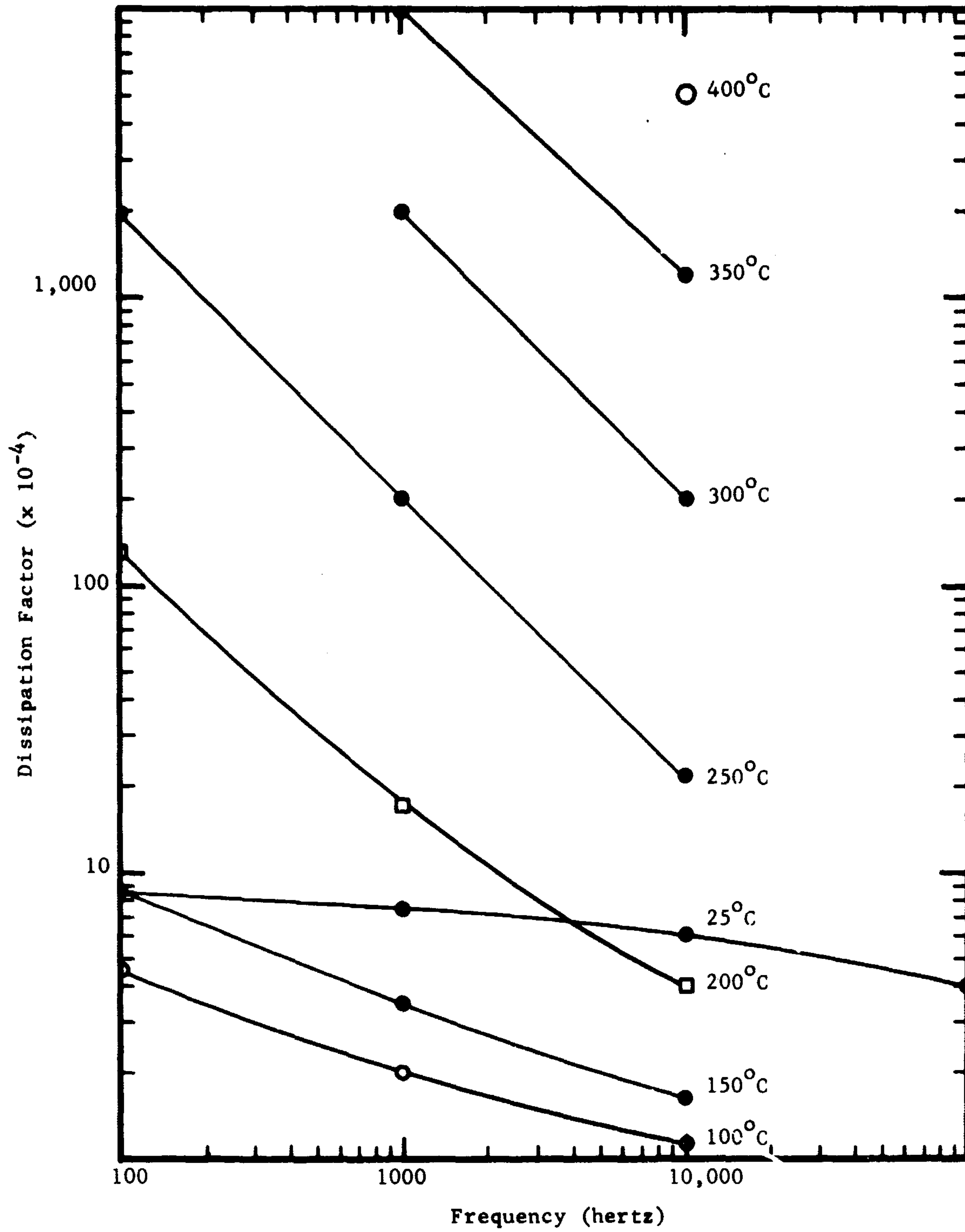

FIGURE 21. THE EFFECT OF FREQUENCY AND TEMPERATURE ON THE DISSIPATION FACTOR OF FUSED QUARTZ

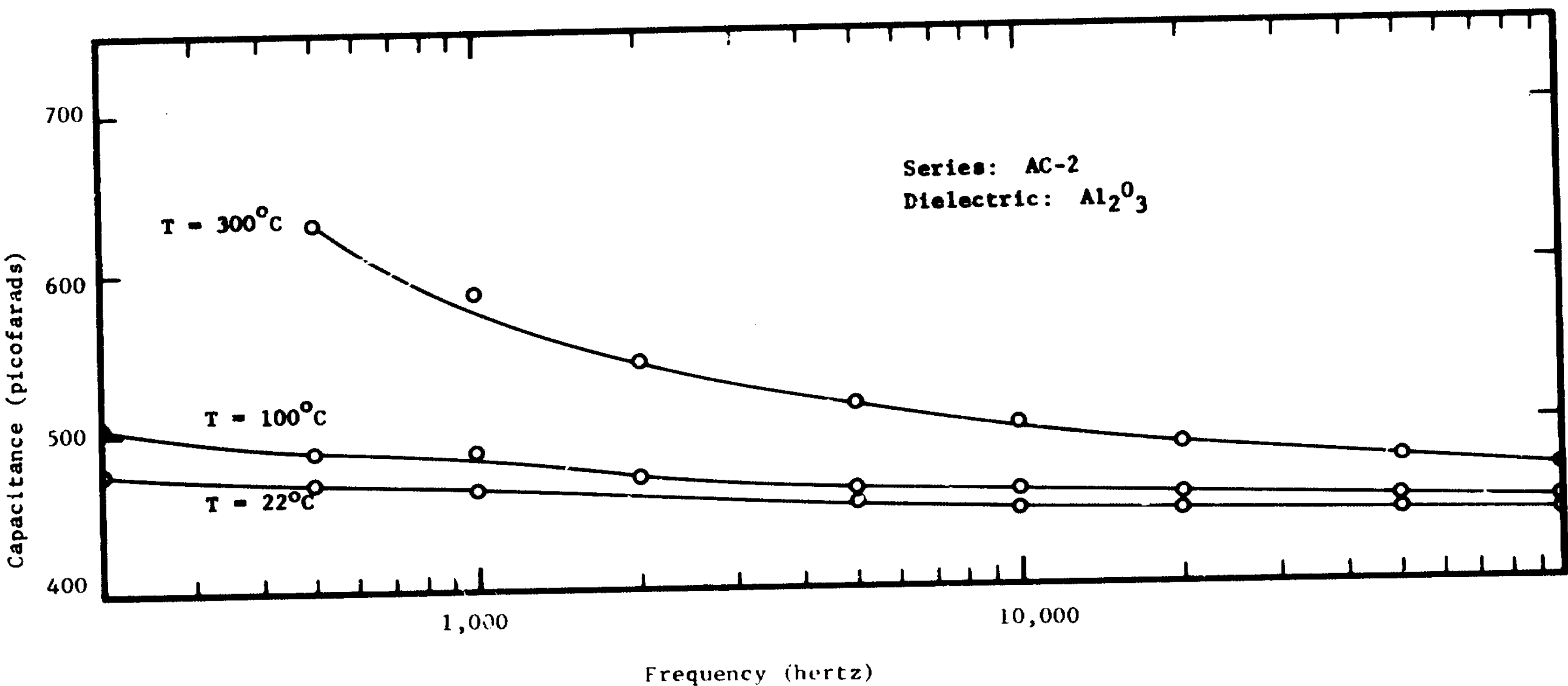

FIGURE 22. THE EFFECT OF FREQUENCY AND TEMPERATURE ON CAPACITANCE OF SERIES AC THIN FILM CAPACITORS

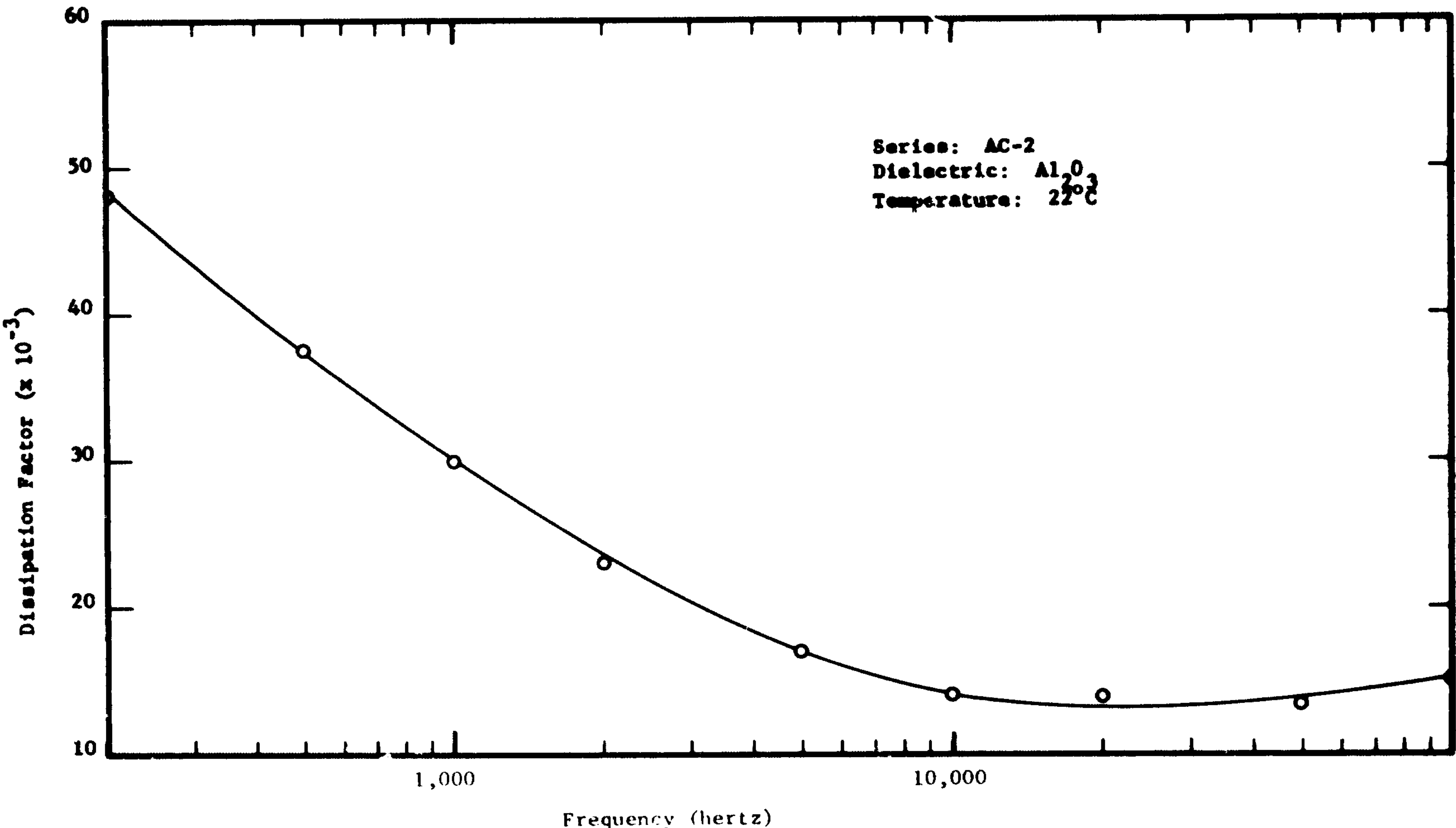

FIGURE 23. THE EFFECT OF FREQUENCY DISSIPATION FACTOR OF SERIES AC THIN FILM CAPACITORS

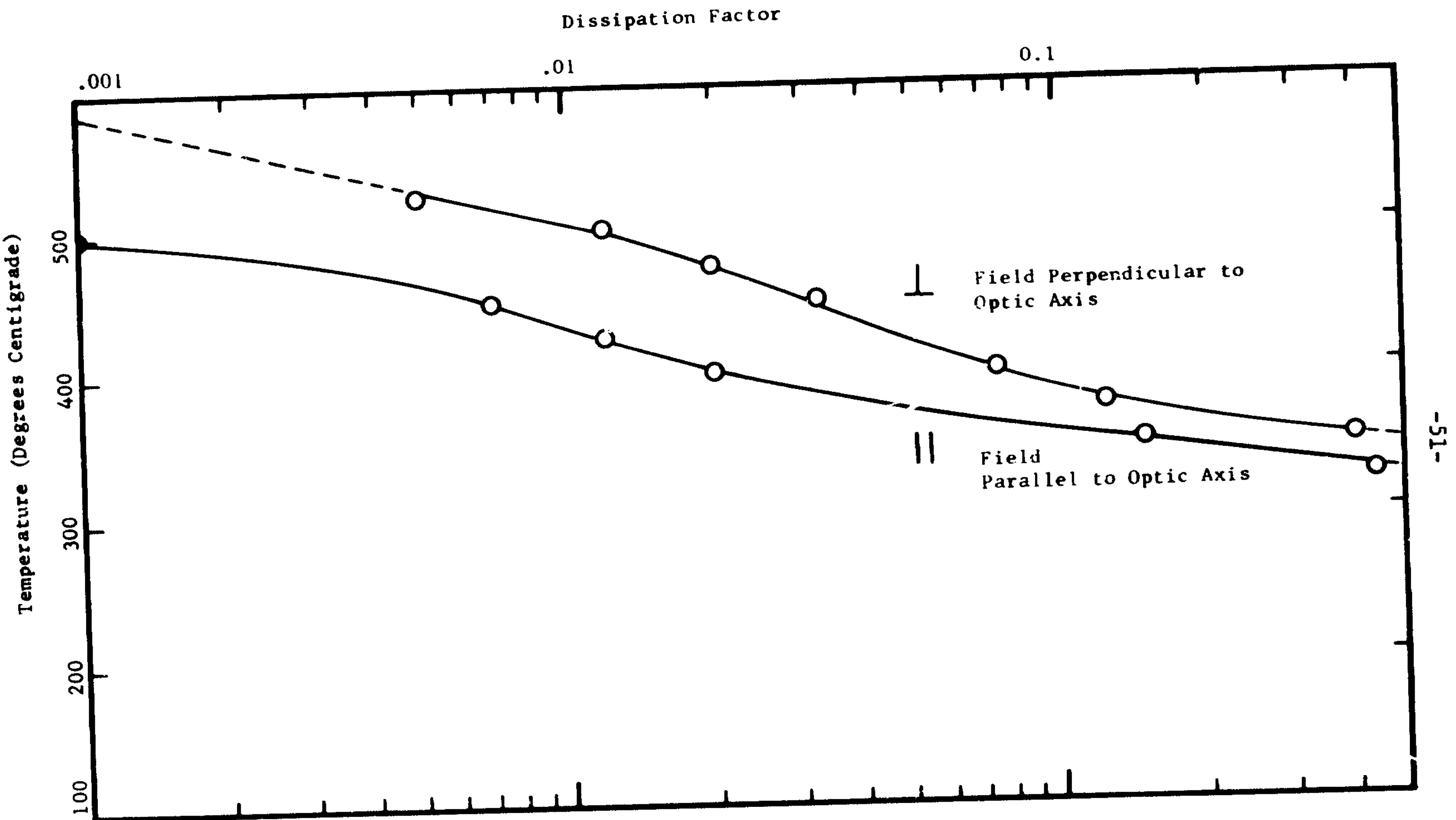

FIGURE 24. THE EFFECT OF TEMPERATURE ON THE DISSIPATION FACTOR OF Al_2O_3 AT A FREQUENCY OF 1 kHz

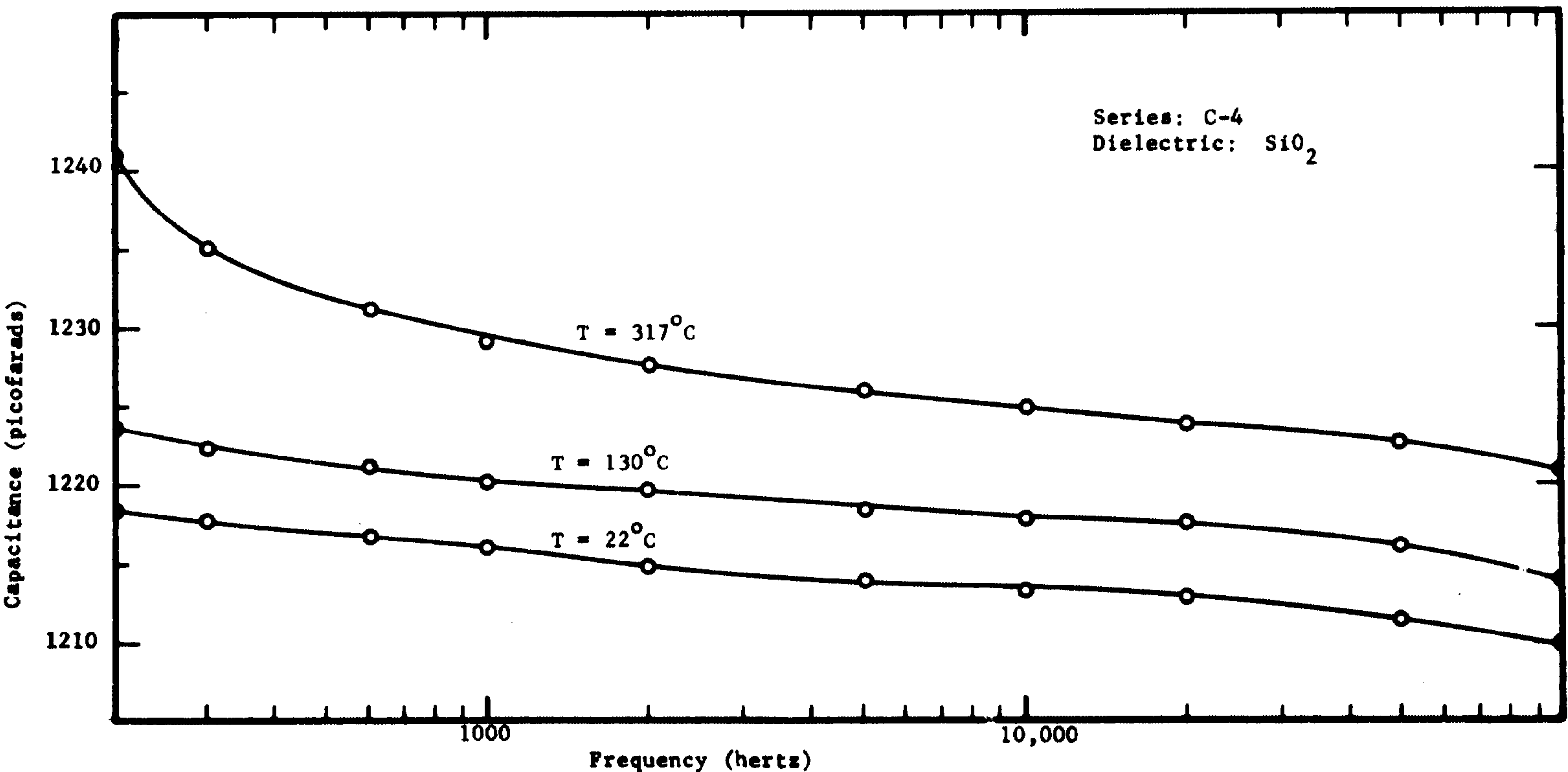

FIGURE 25. EFFECT OF FREQUENCY AND TEMPERATURE ON CAPACITANCE OF SERIES C-4 THIN FILM CAPACITORS

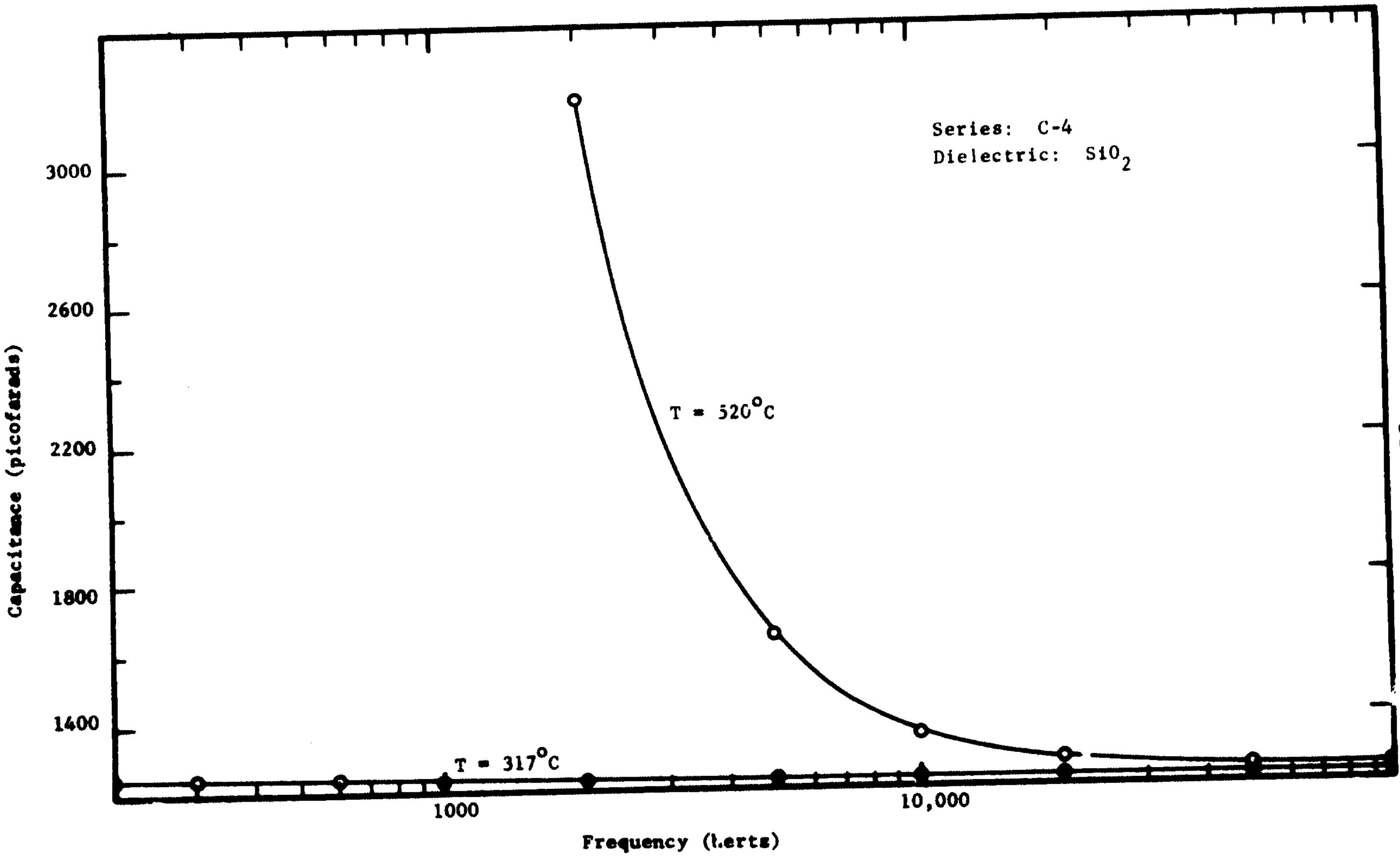

FIGURE 26. EFFECT OF FREQUENCY AND TEMPERATURE ON CAPACITANCE OF SERIES C-4 THIN FILM CAPACITORS

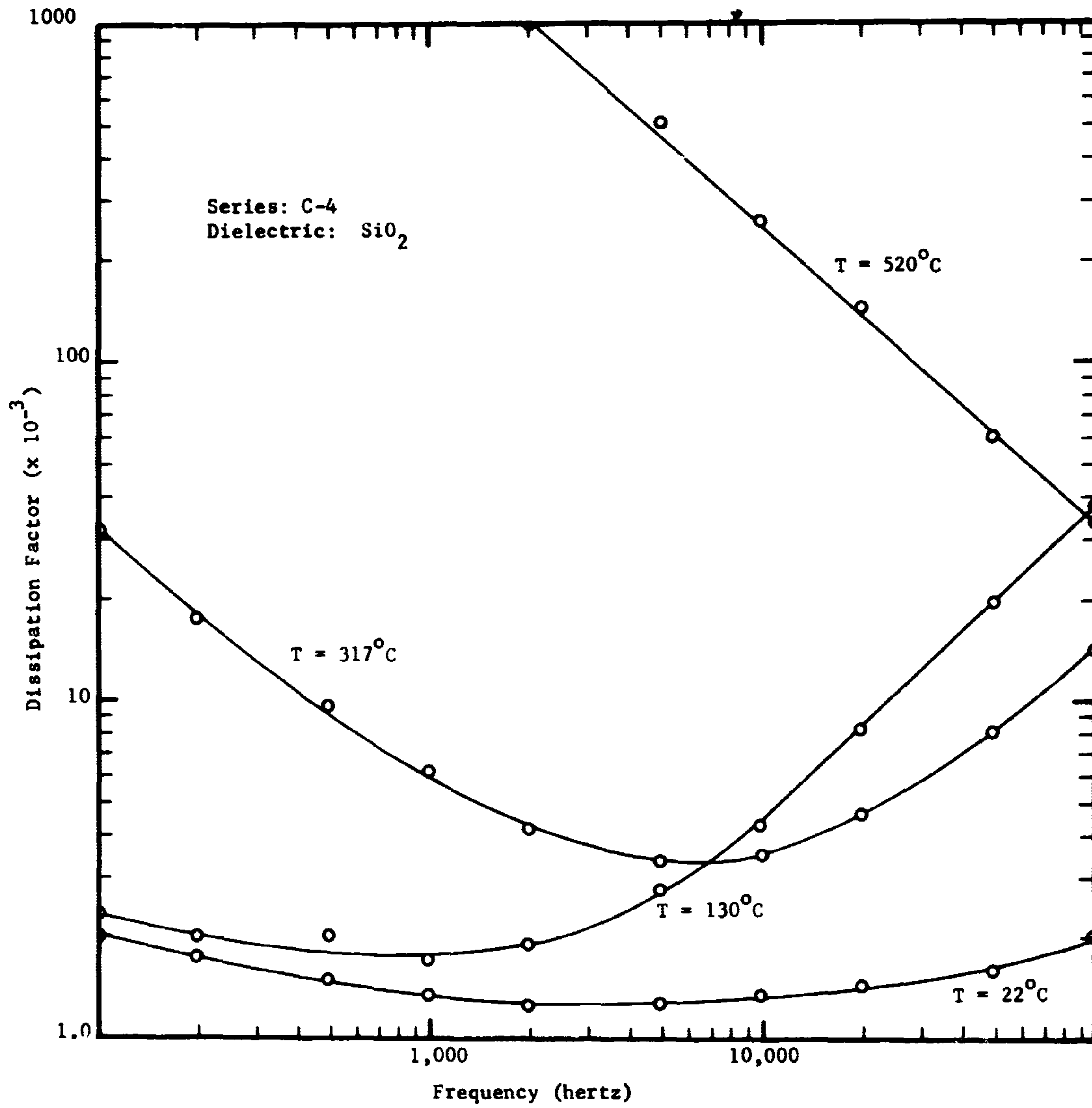

FIGURE 27. EFFECT OF FREQUENCY AND TEMPERATURE ON DISSIPATION FACTOR OF SERIES C-4 THIN FILM CAPACITORS

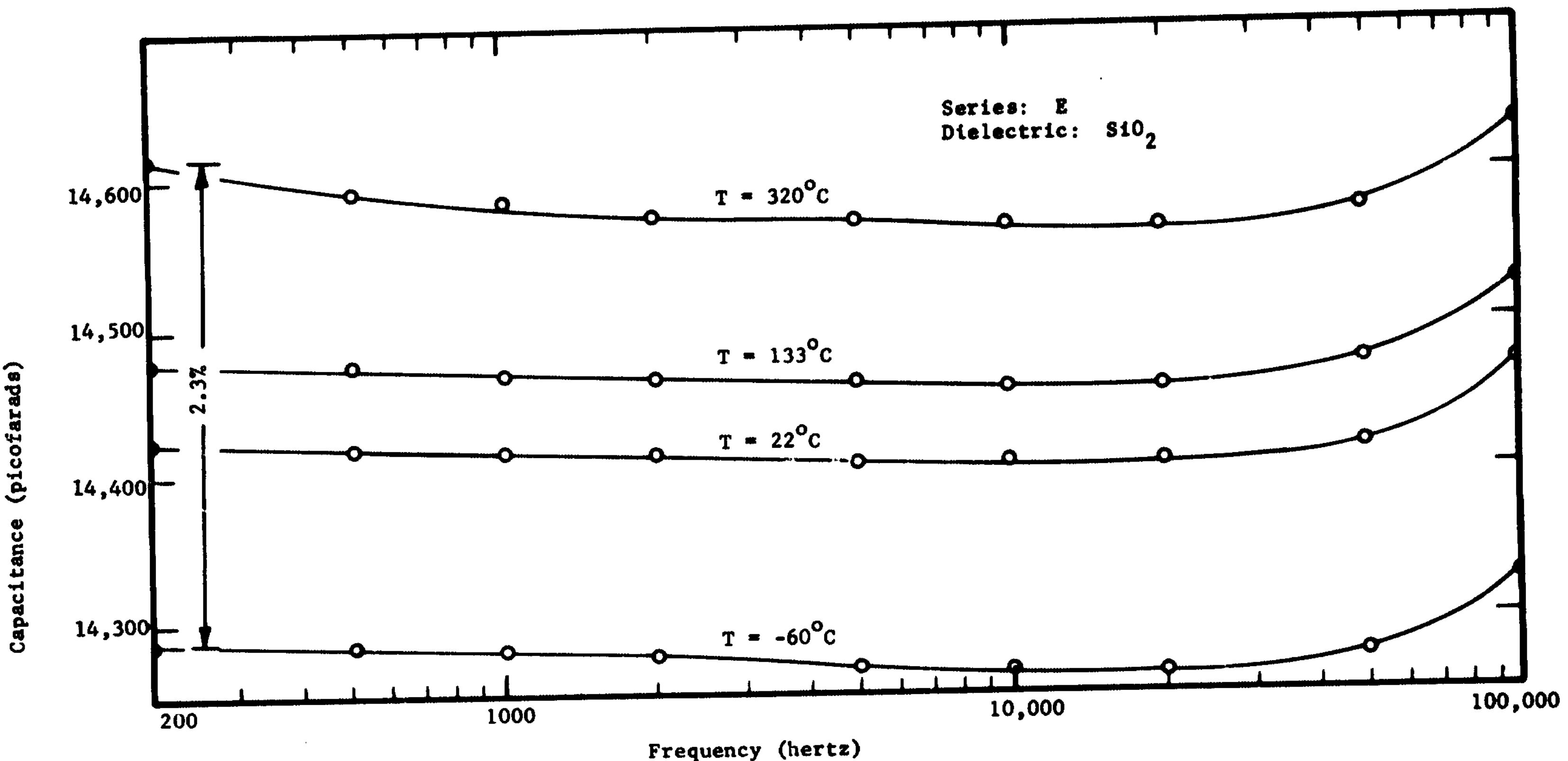

FIGURE 28. EFFECT OF FREQUENCY AND TEMPERATURE ON CAPACITANCE OF SERIES E THIN FILM CAPACITORS

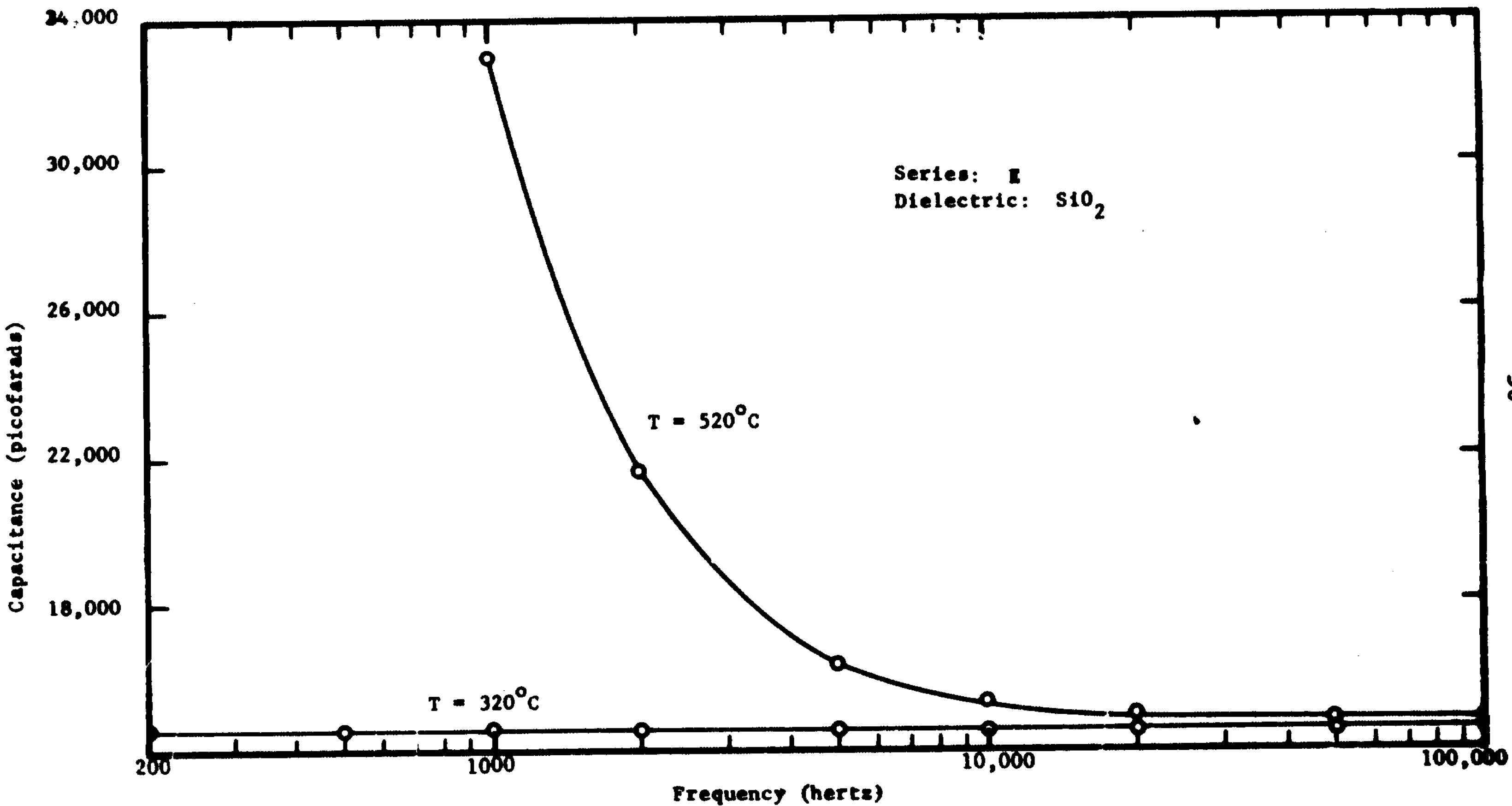

FIGURE 29. EFFECT OF FREQUENCY AND TEMPERATURE ON CAPACITANCE OF SERIES E THIN FILM CAPACITORS

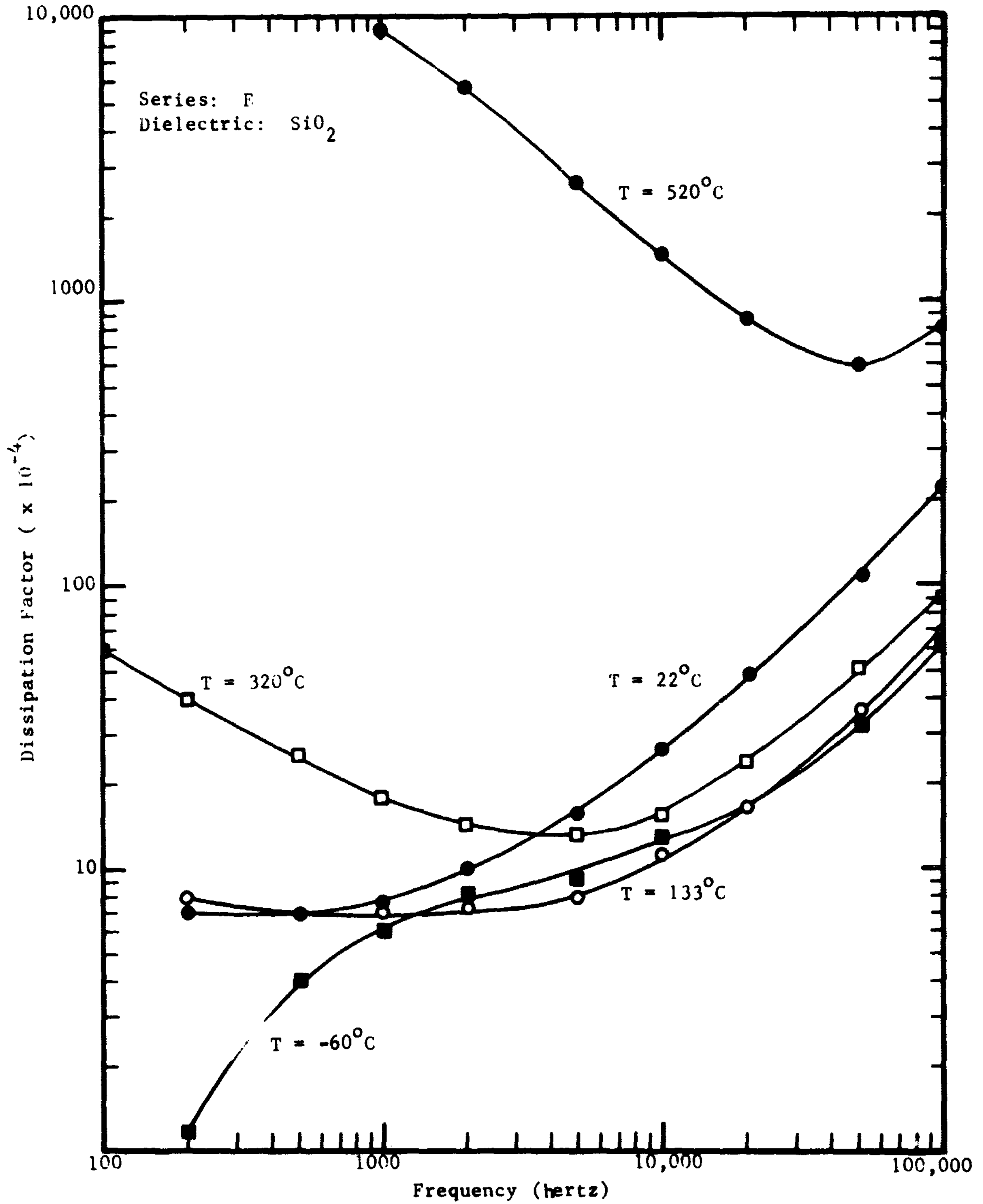

FIGURE 30. EFFECT OF FREQUENCY AND TEMPERATURE ON THE DISSIPATION FACTOR OF SERIES E THIN FILM CAPACITORS

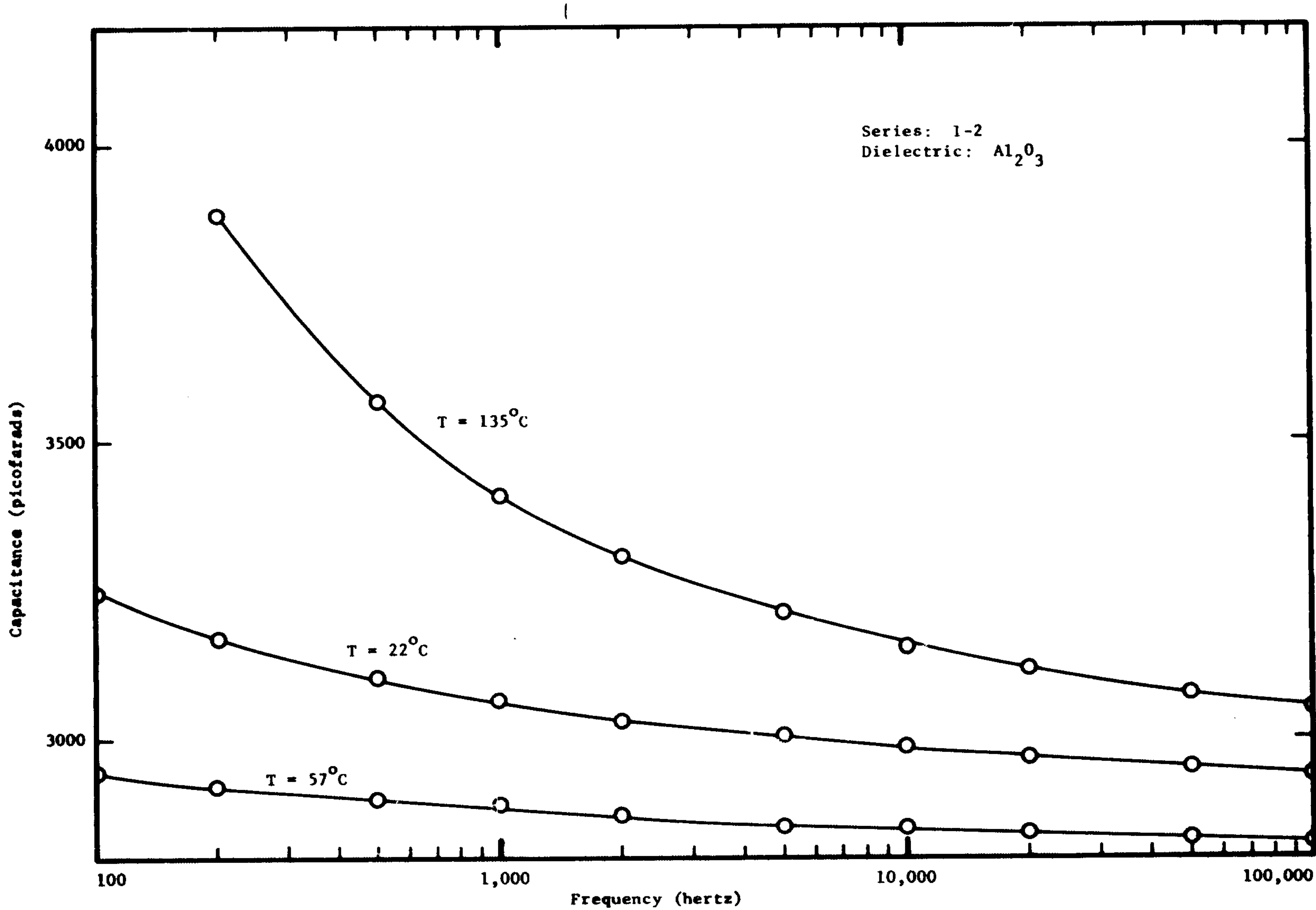

FIGURE 31. THE EFFECT OF FREQUENCY AND TEMPERATURE ON CAPACITANCE OF SERIES I-2 THIN FILM CAPACITORS

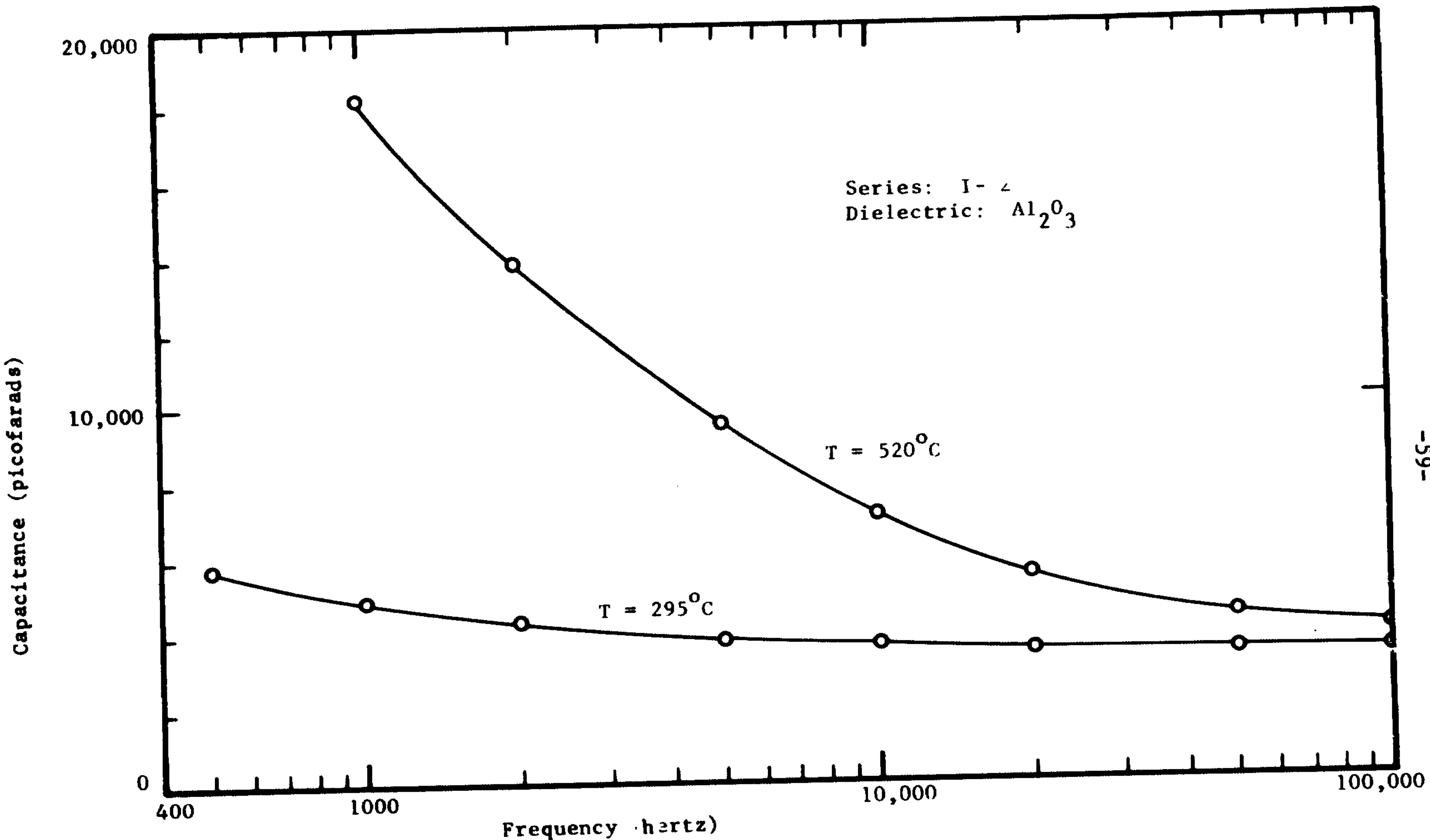

FIGURE 32. EFFECT OF FREQUENCY AND TEMPERATURE ON CAPACITANCE OF SERIES I-2 THIN FILM CAPACITORS

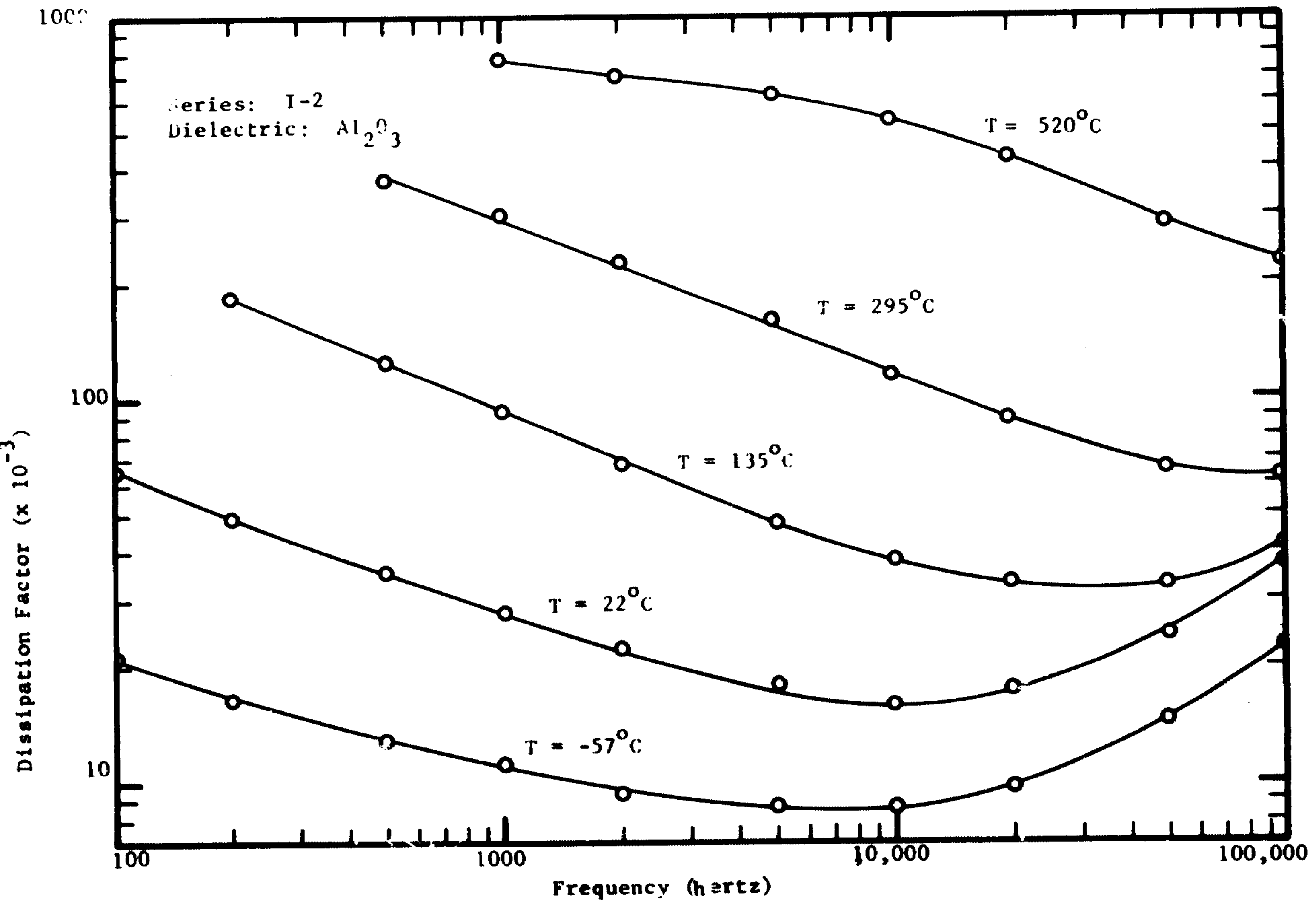

FIGURE 33. EFFECT OF FREQUENCY AND TEMPERATURE ON DISSIPATION FACTOR OF SERIES I-2 THIN FILM CAPACITORS

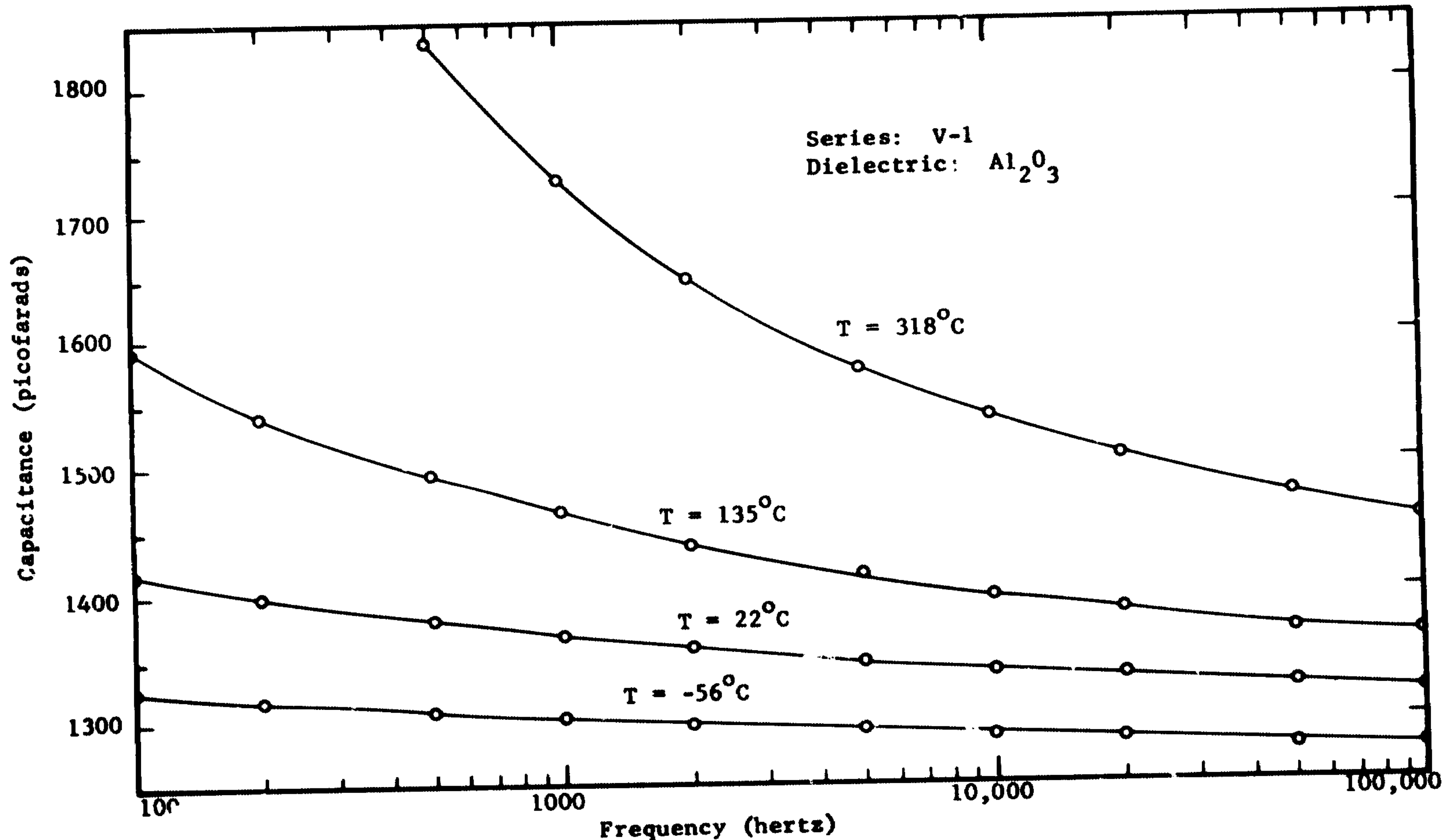

FIGURE 34. EFFECT OF FREQUENCY AND TEMPERATURE ON CAPACITANCE OF SERIES V-1 THIN FILM CAPACITOR

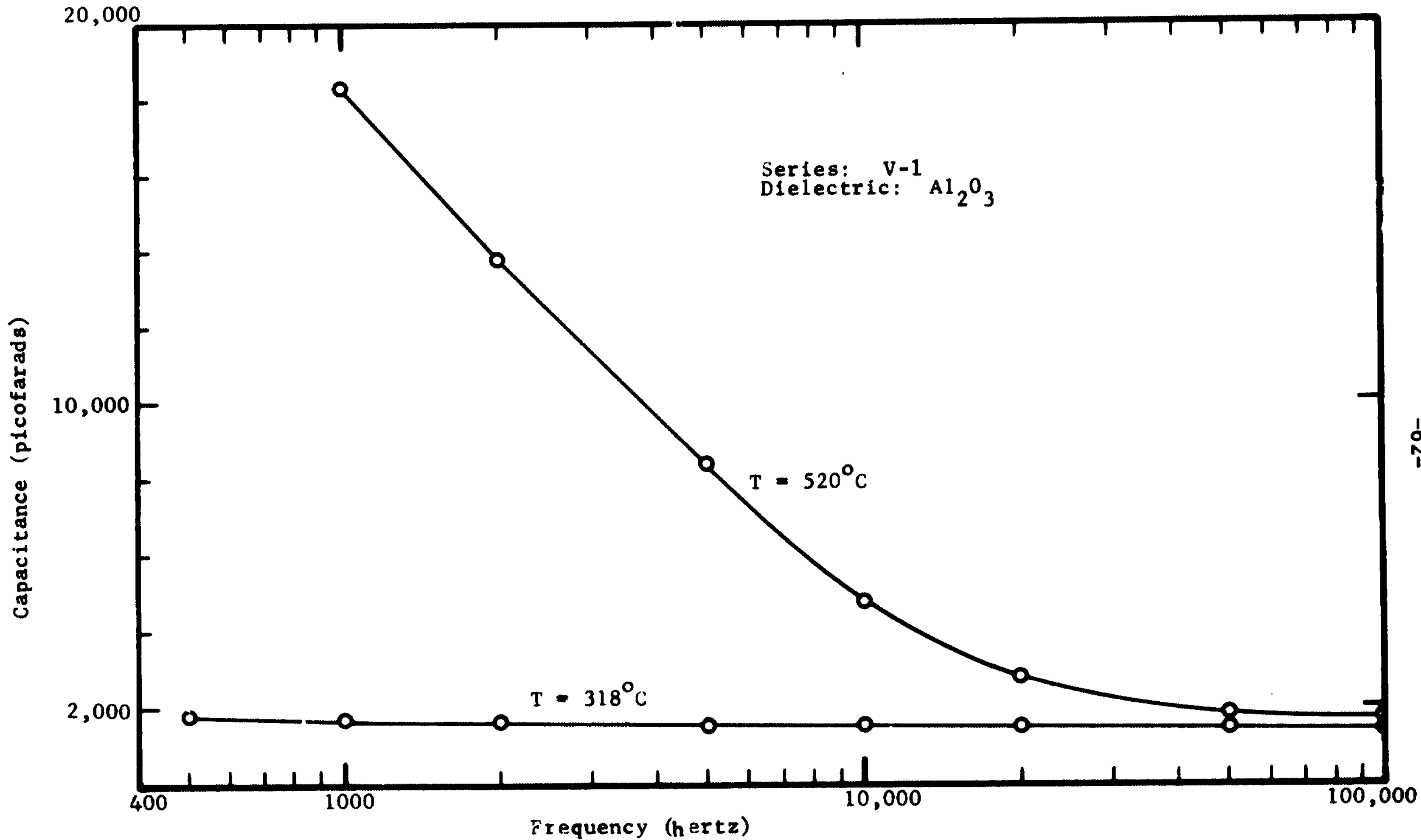

FIGURE 35. EFFECT OF FREQUENCY AND TEMPERATURE ON CAPACITANCE OF SERIES V-1 THIN FILM CAPACITORS

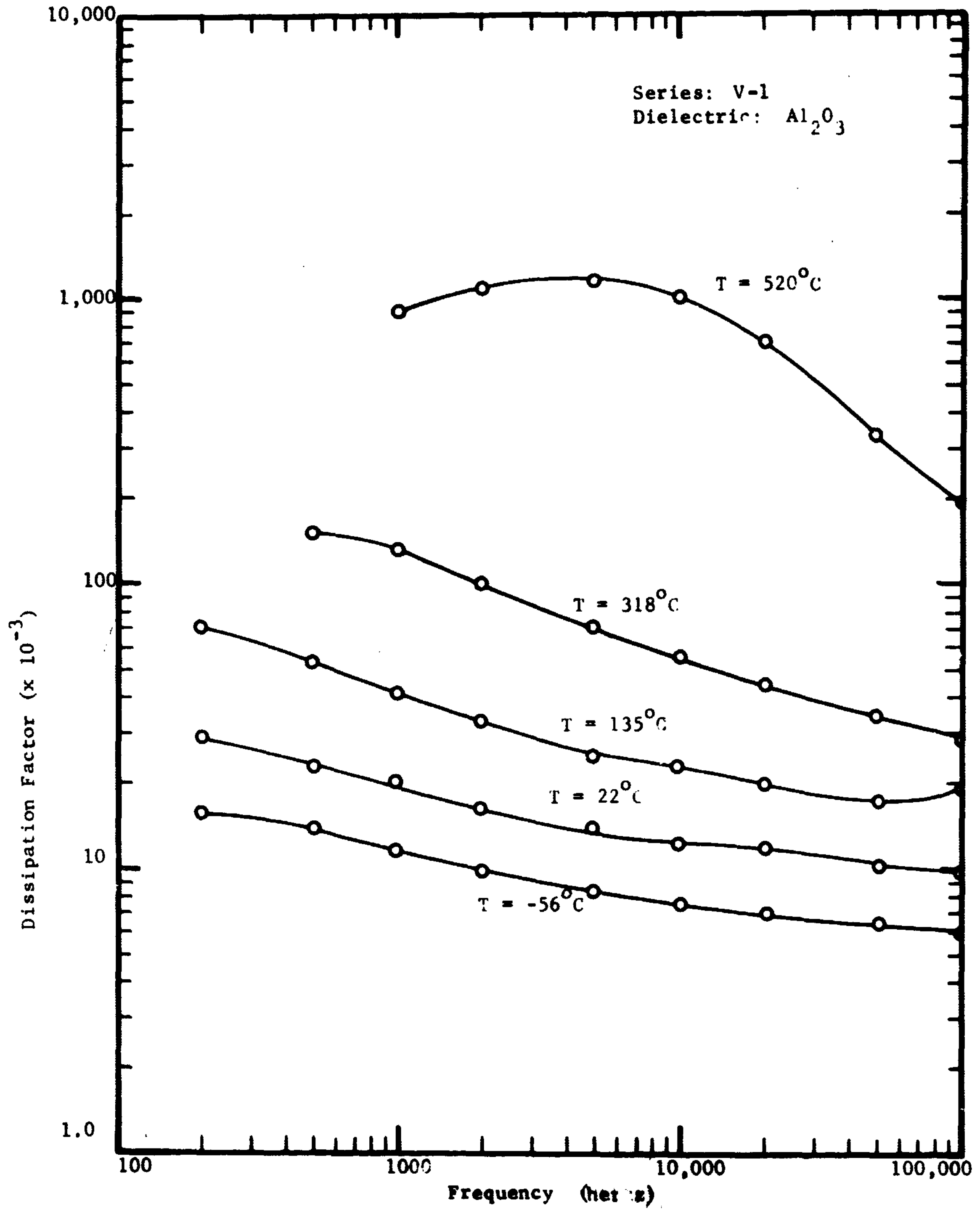

FIGURE 36. EFFECT OF FREQUENCY AND TEMPERATURE ON DISSIPATION FACTOR OF SERIES V-1 THIN FILM CAPACITORS

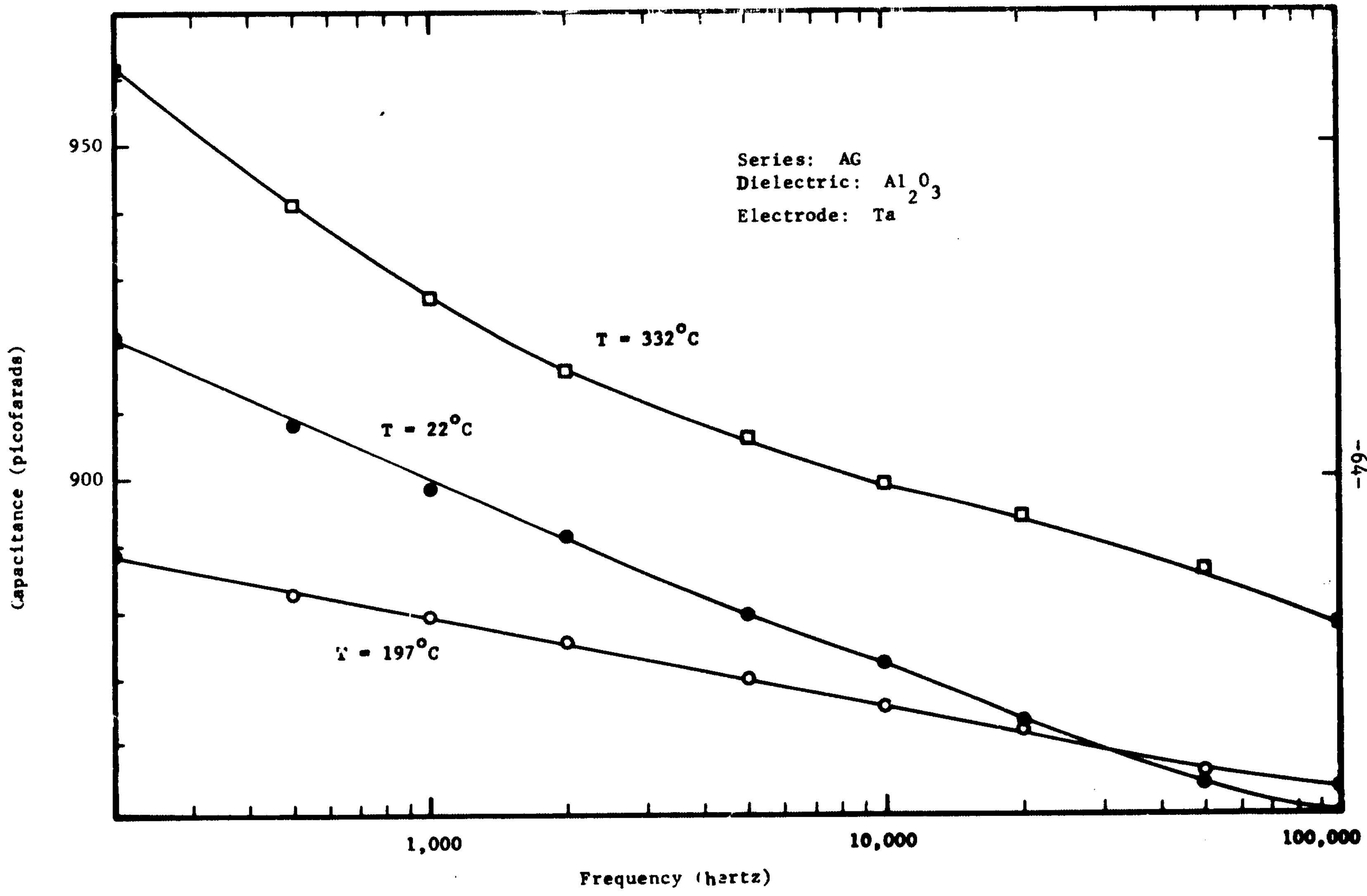

FIGURE 37. EFFECT OF FREQUENCY AND TEMPERATURE ON CAPACITANCE OF SERIES AG THIN FILM CAPACITORS

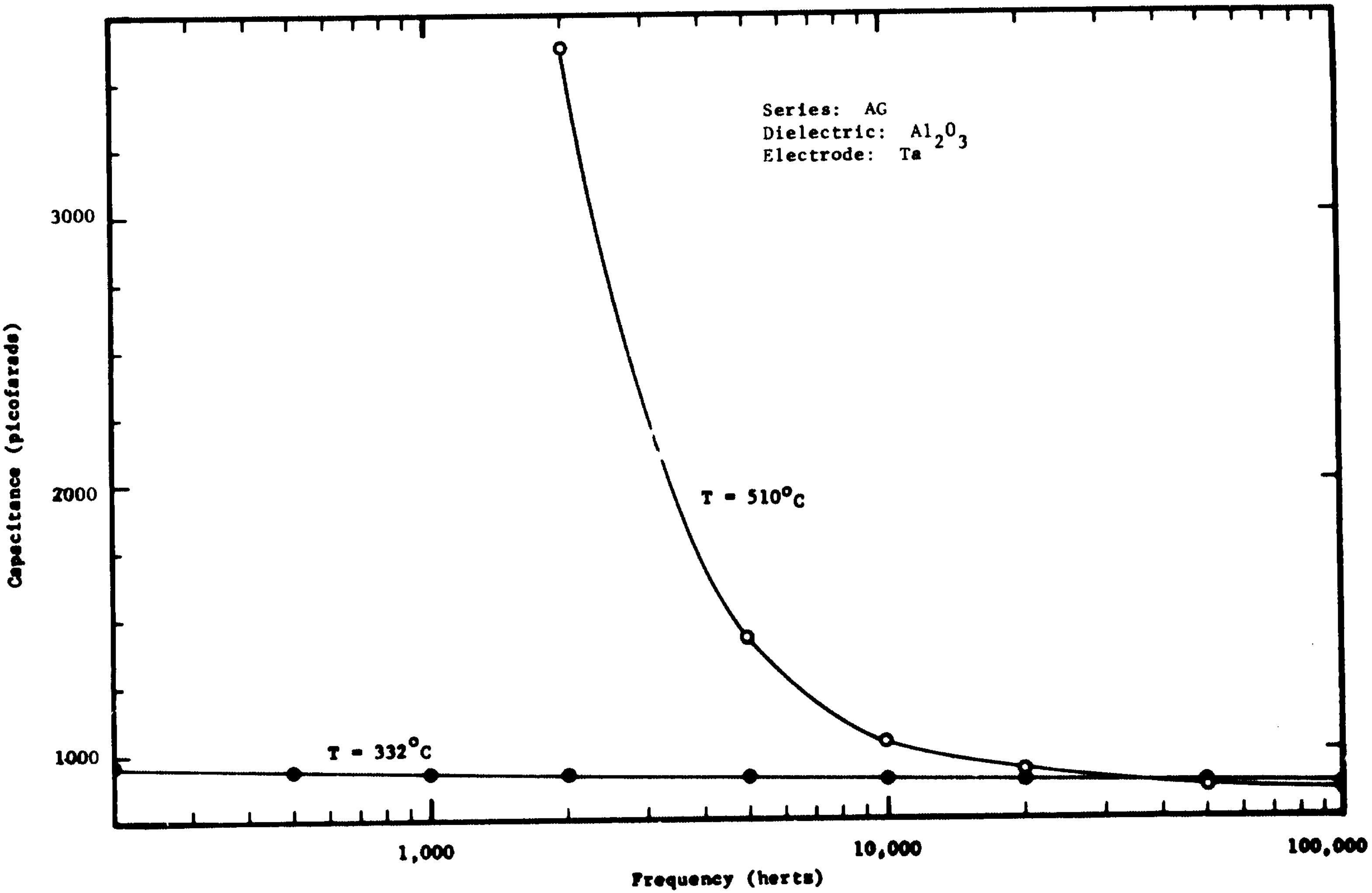

FIGURE 38. EFFECT OF FREQUENCY AND TEMPERATURE ON CAPACITANCE OF SERIES AG THIN FILM CAPACITORS

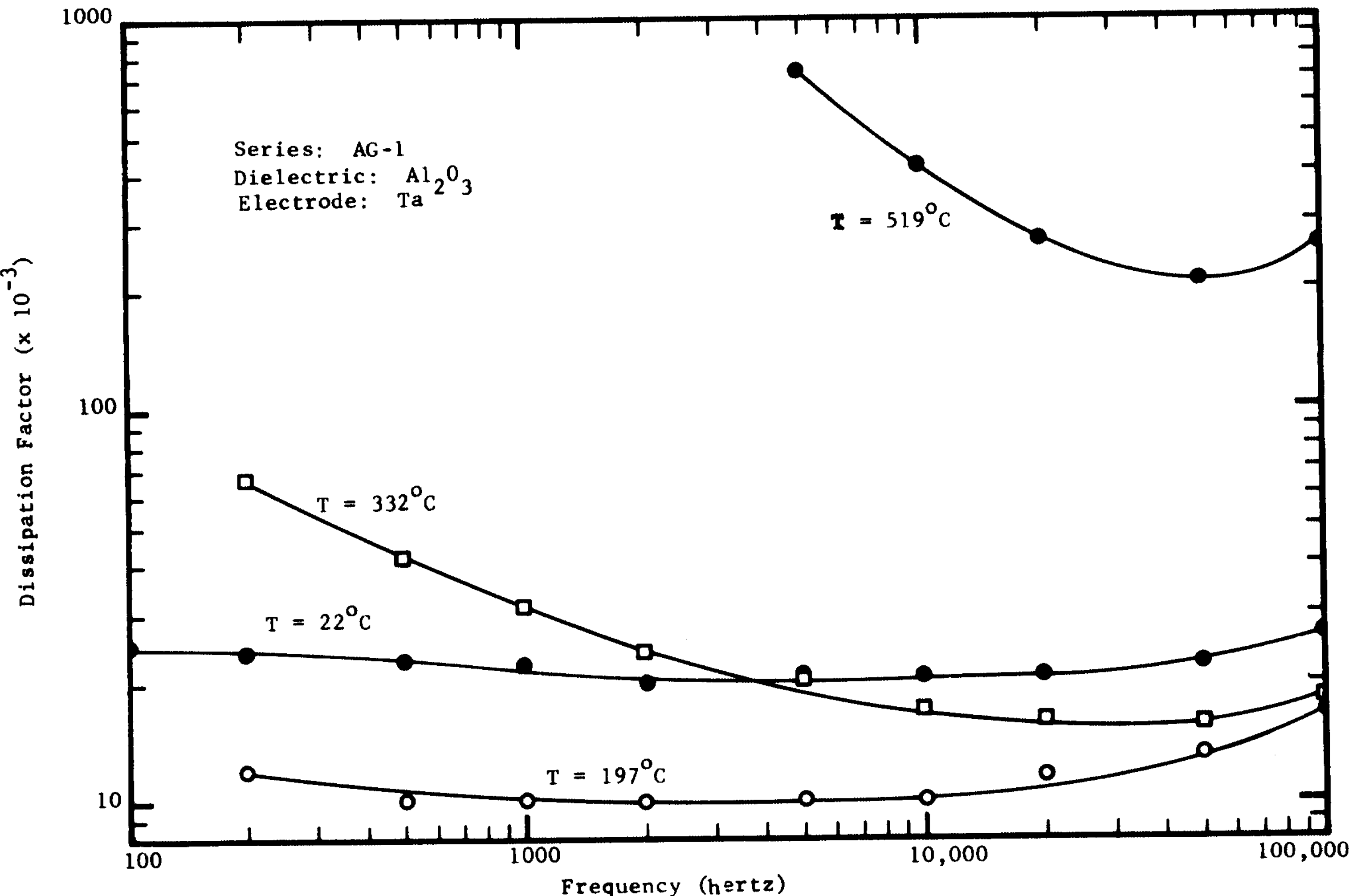

FIGURE 39. THE EFFECT OF TEMPERATURE AND FREQUENCY ON DISSIPATION FACTOR OF SERIES AG-1 CAPACITORS

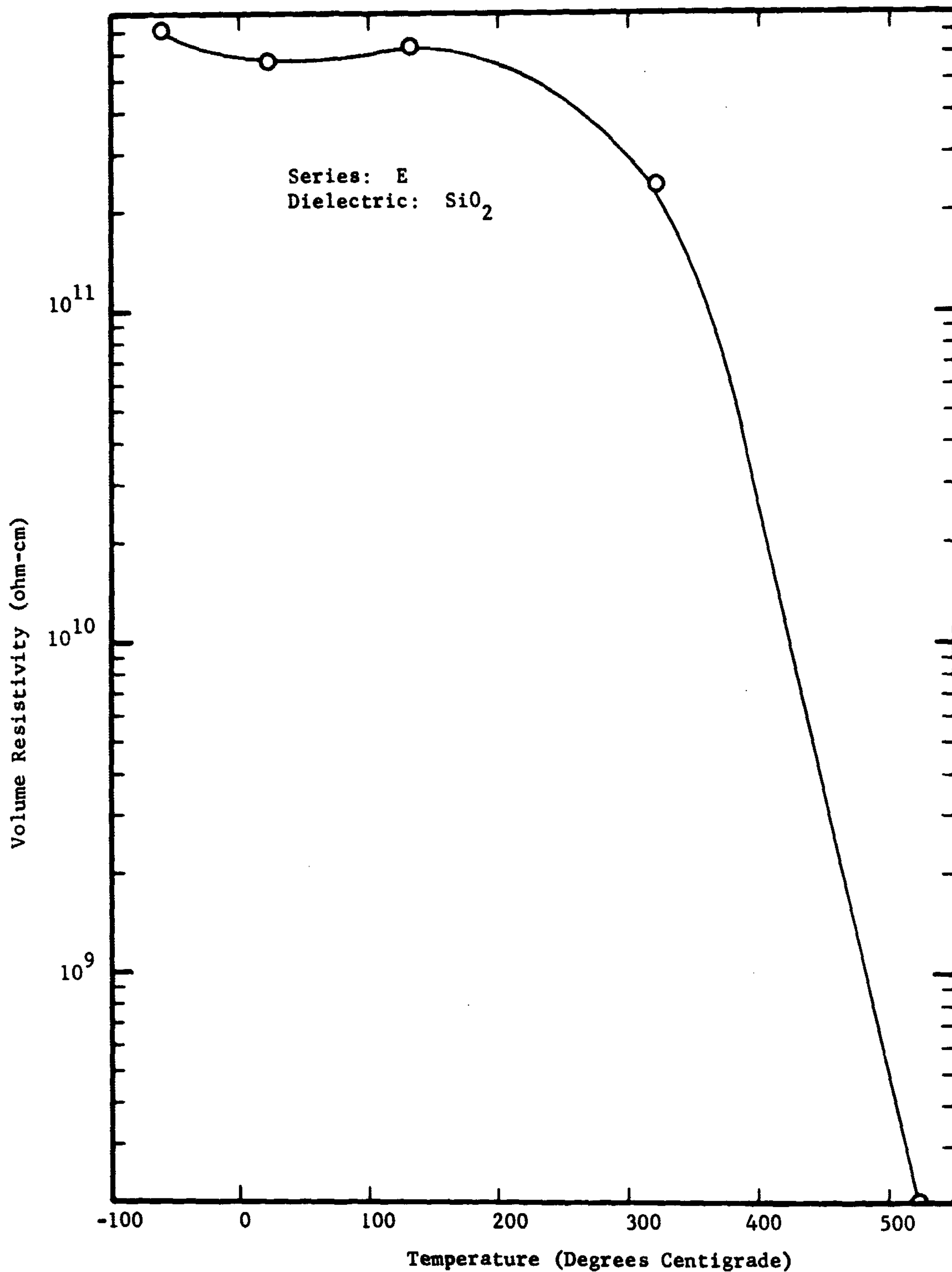

FIGURE 40. VOLUME RESISTIVITY VERSUS TEMPERATURE AT 1 kHz FREQUENCY OF SERIES E CAPACITORS

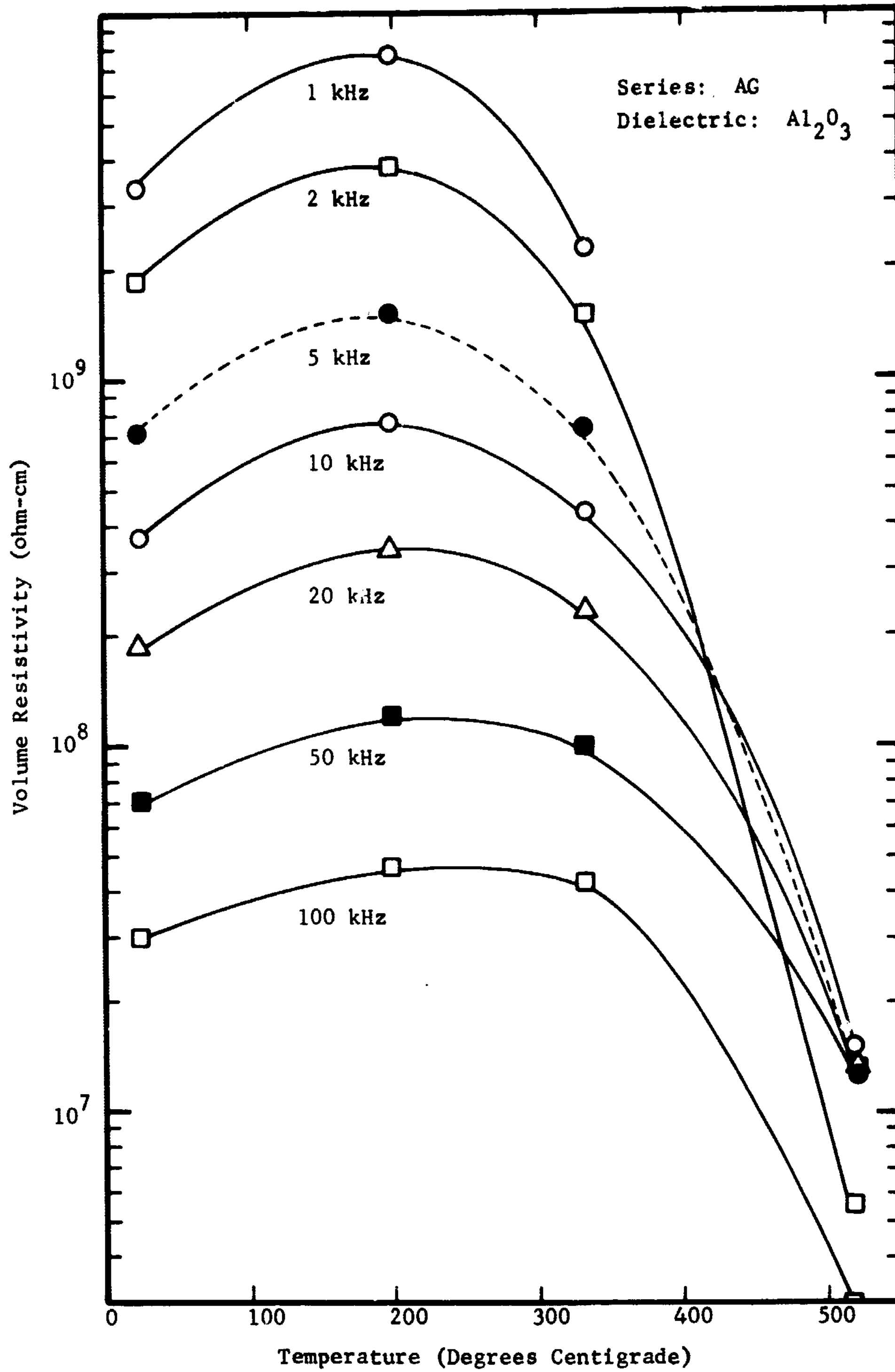

FIGURE 41. THE EFFECT OF TEMPERATURE AND FREQUENCY ON VOLUME RESISTIVITY OF SERIES AG CAPACITORS

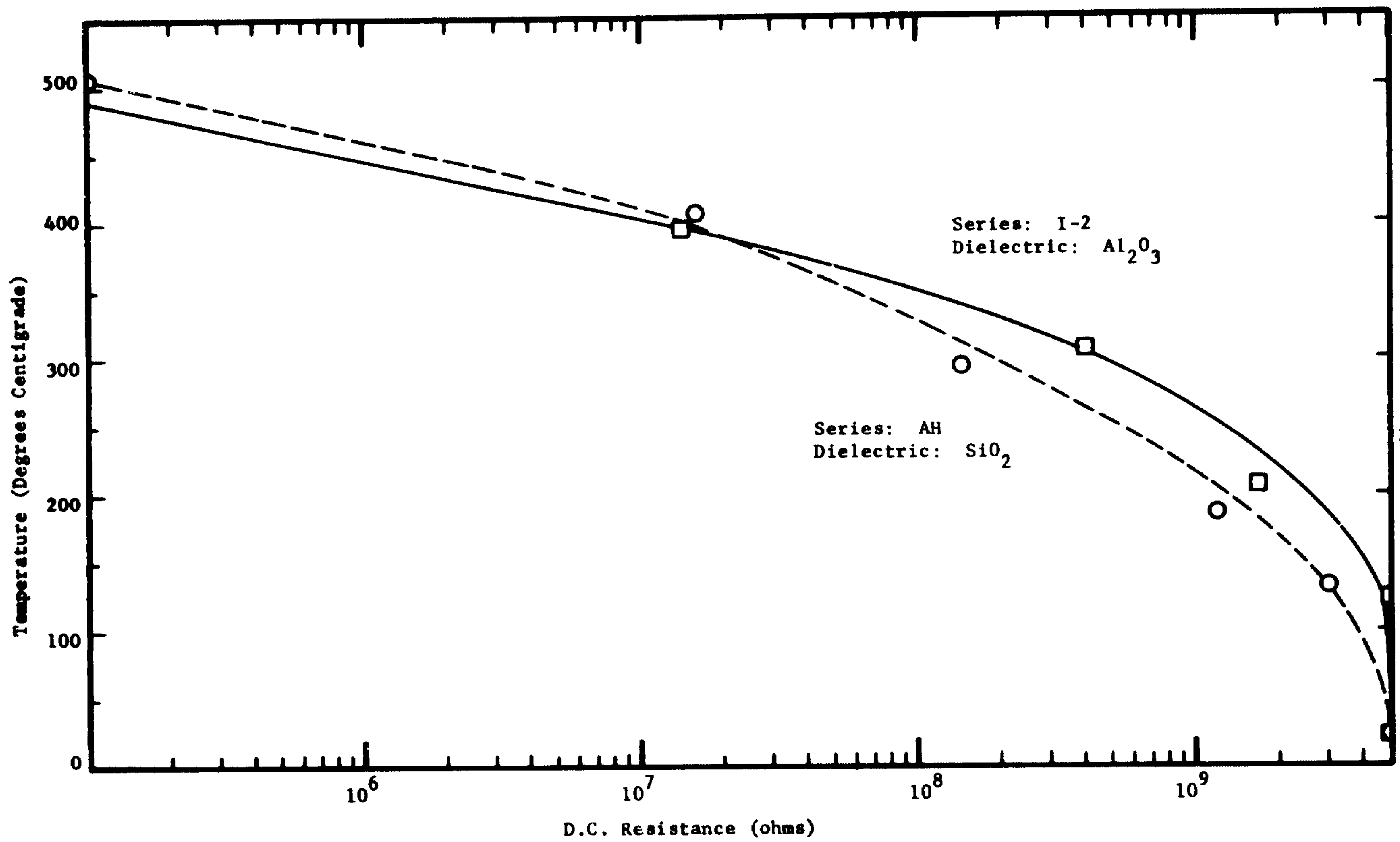

FIGURE 42. THE EFFECT OF TEMPERATURE ON D.C. RESISTANCE OF Al_2O_3 AND SiO_2 CAPACITORS

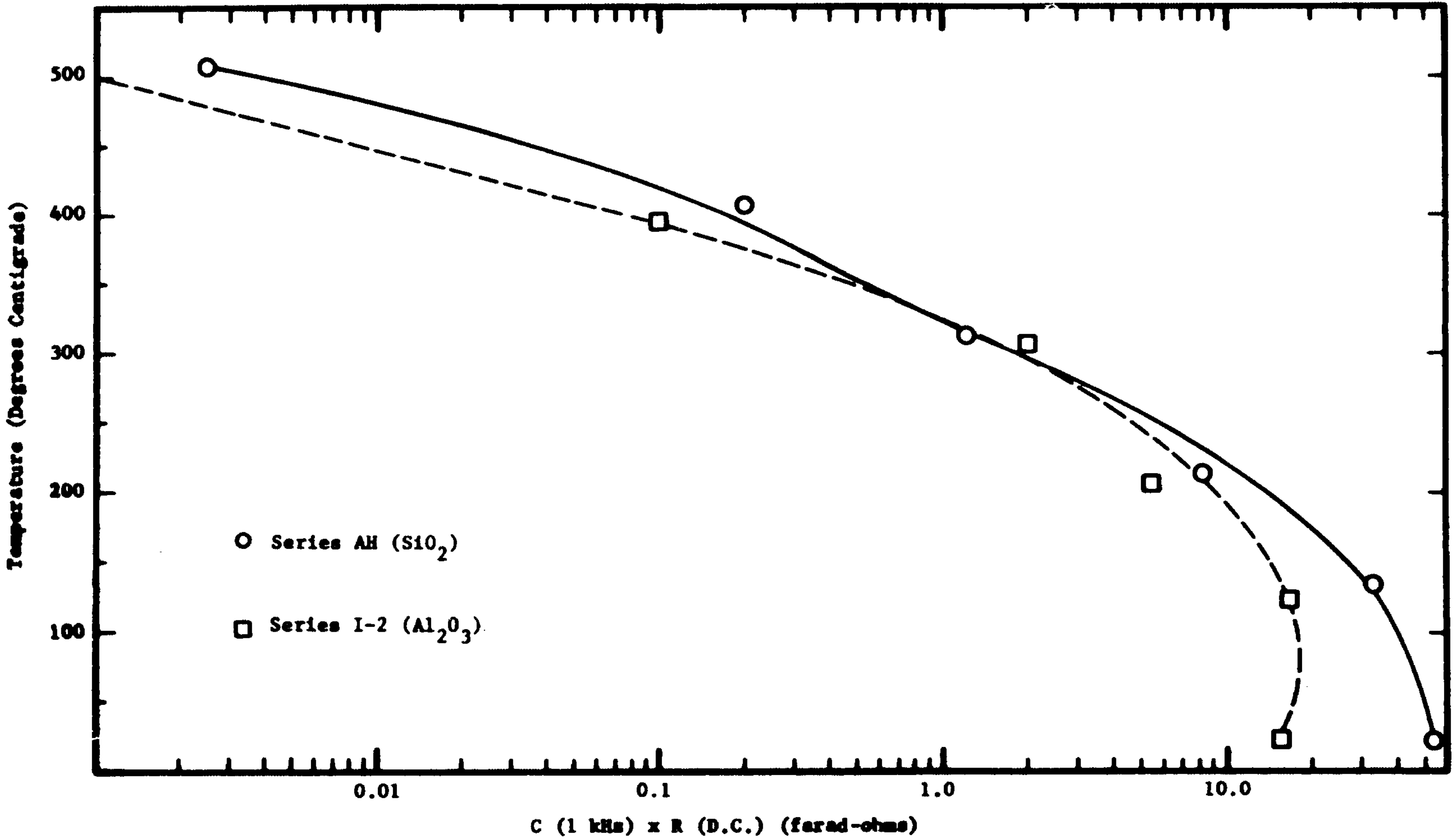

FIGURE 43. THE EFFECT OF TEMPERATURE ON THE C (1 kHz) x R (D.C.) PRODUCT

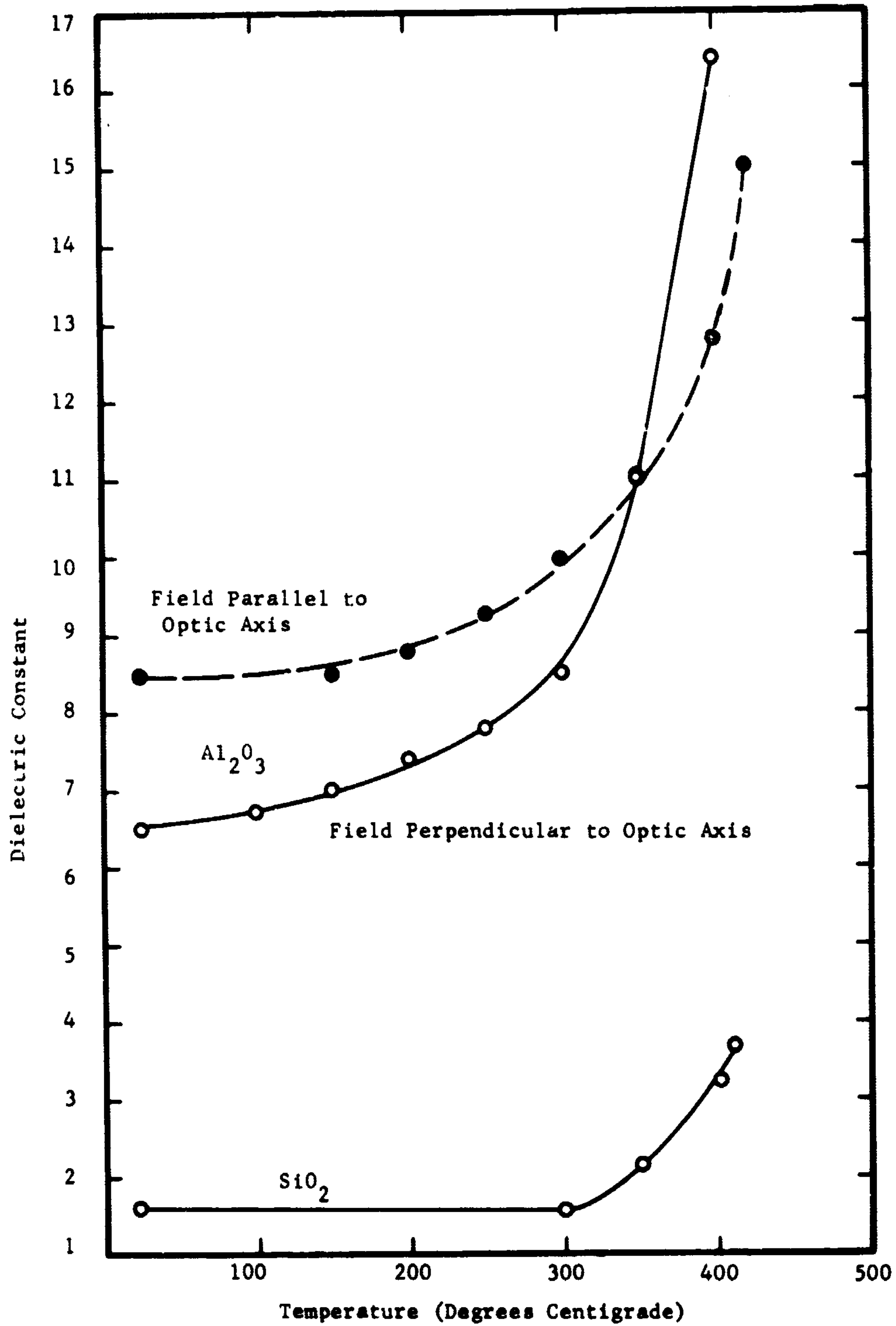

FIGURE 44. THE EFFECT OF TEMPERATURE ON THE DIELECTRIC CONSTANT OF BULK SiO_2 AND Al_2O_3 (FREQUENCY - 1 kHz)

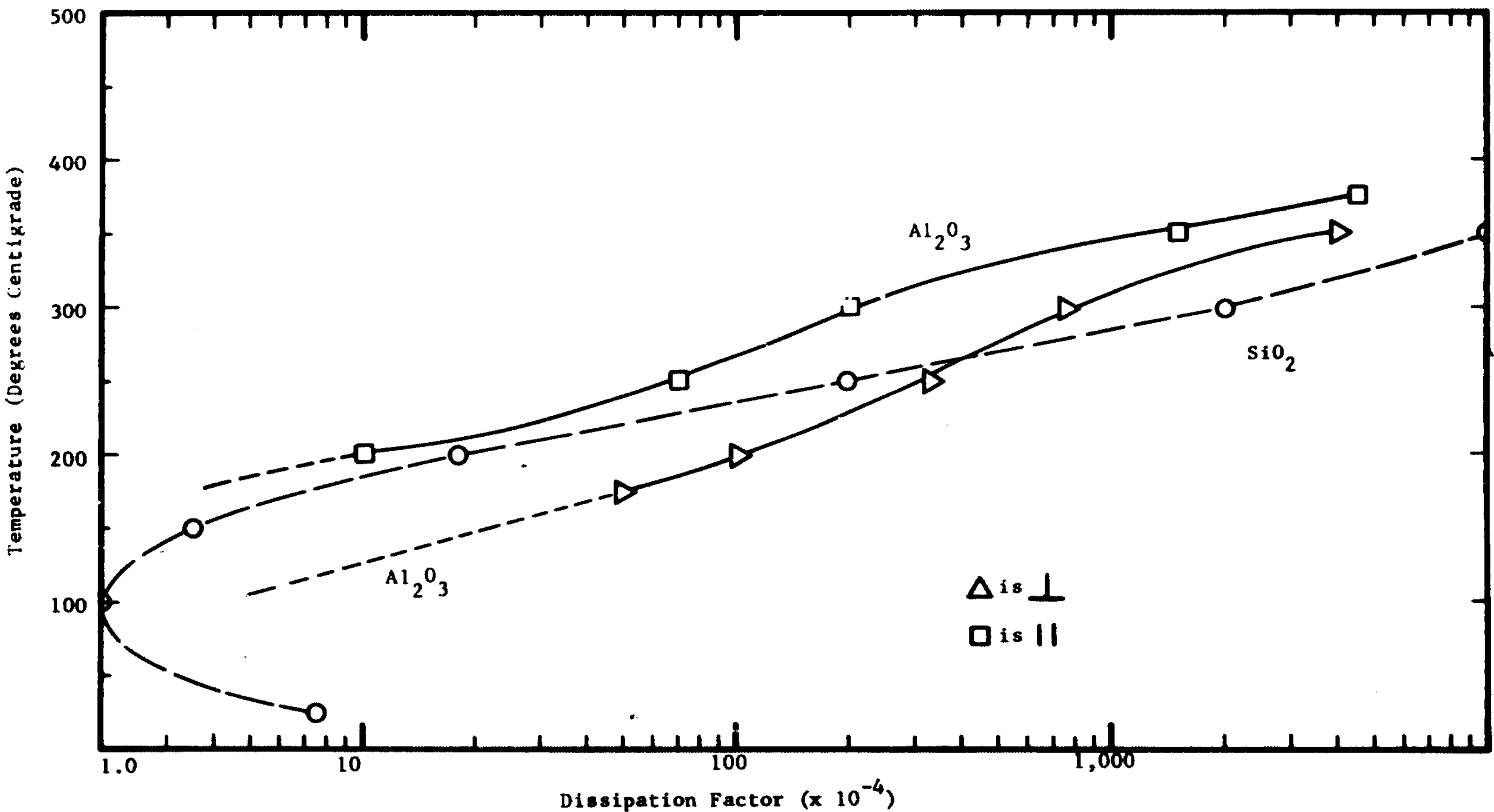

FIGURE 45. THE EFFECT OF TEMPERATURE ON THE BULK DISSIPATION FACTOR OF Al_2O_3 AND SiO_2 (FREQUENCY - 1 kHz)

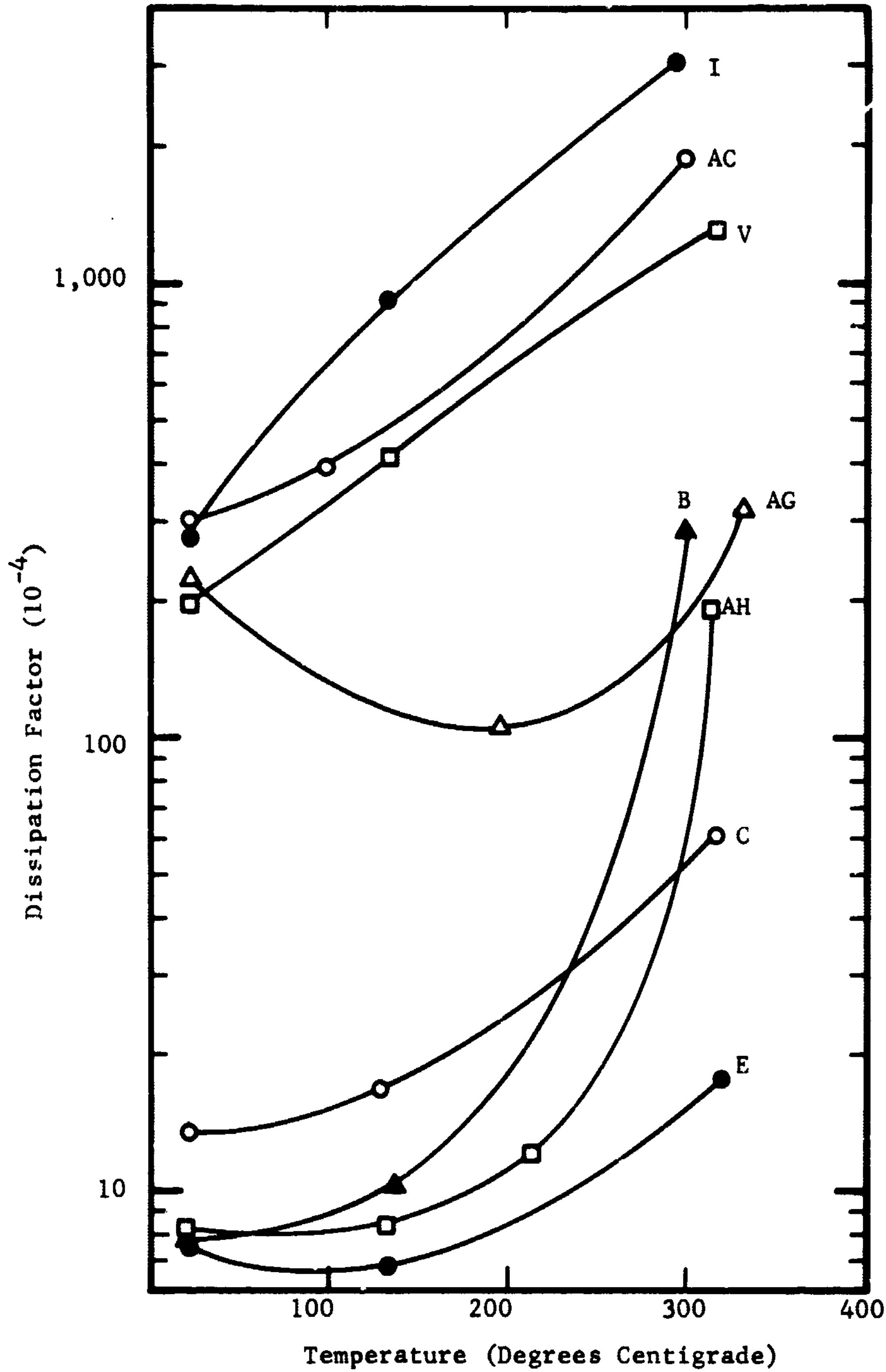

FIGURE 46. THE EFFECT OF TEMPERATURE ON DISSIPATION FACTOR OF VARIOUS CAPACITOR SYSTEMS (Frequency = 1 kHz)

APPENDIX

New Technology Appendix

"After a diligent review of the work performed under this contract, no new innovation, discovery, improvement or invention was conceived worthy of reporting at the time of publication".

The equivalent electrical circuit of a capacitor is shown in Figure 12 and the terminal impedence is,

$$Z_t = (R + j\omega L) + \frac{1}{G+j\omega C} \tag{A-1}$$

Rearranging Equation (A-1) into real and imaginary components results in,

$$Z_t = \left[R + \frac{G}{\omega^2C^2+G^2}\right] + j\left[\omega L - \frac{\omega C}{\omega^2C^2+G^2}\right] \tag{A-2}$$

For,

$$G^2 << \omega^2C^2$$

the effective terminal capacitance (C_t) can be determined,

$$-\frac{1}{\omega C_t} = \omega L - \frac{1}{\omega C} \tag{A-3}$$

and

$$C_t = \frac{C}{1-\omega^2LC} \tag{A-4}$$

The dissipation factor (D) of the capacitor is the ratio of the magnitudes of the real and imaginary parts of Equation (A-2). At low frequencies, (L = 0), and for $G^2 << \omega^2C^2$,

$$D = \omega CR = \frac{G}{\omega C} \tag{A-5}$$